The Journal of Chemical Physics

Vibrationally excited states of 1*H*- and 2*H*-1,2,3-triazole isotopologues analyzed by millimeter-wave and high-resolution infrared spectroscopy with approximate state-specific quartic distortion constants

Cite as: J. Chem. Phys. **158**, 044301 (2023); https://doi.org/10.1063/5.0137340
Submitted: 01 December 2022 • Accepted: 02 January 2023 • Published Online: 25 January 2023

Maria A. Zdanovskaia, Peter R. Franke, Brian J. Esselman, et al.

The Journal of Chemical Physics ARTICLE scitation.org/journal/jcp

Vibrationally excited states of 1*H*- and 2*H*-1,2,3-triazole isotopologues analyzed by millimeter-wave and high-resolution infrared spectroscopy with approximate state-specific quartic distortion constants

Cite as: J. Chem. Phys. 158, 044301 (2023); doi: 10.1063/5.0137340
Submitted: 1 December 2022 • Accepted: 2 January 2023 •
Published Online: 25 January 2023

Maria A. Zdanovskaia,[1] Peter R. Franke,[2] Brian J. Esselman,[1] Brant E. Billinghurst,[3] Jianbao Zhao,[3] John F. Stanton,[2,a)] R. Claude Woods,[1,a)] and Robert J. McMahon[1,a)]

AFFILIATIONS

[1] Department of Chemistry, University of Wisconsin–Madison, Madison, Wisconsin 53706, USA
[2] Quantum Theory Project, Departments of Physics and Chemistry, University of Florida, Gainesville, Florida 32611, USA
[3] Canadian Light Source, Inc., University of Saskatchewan, Saskatoon, Saskatchewan S7N 2V3, Canada

[a)] **Authors to whom correspondence should be addressed:** johnstanton@chem.ufl.edu; rcwoods@wisc.edu; and robert.mcmahon@wisc.edu

ABSTRACT

In this work, we present the spectral analysis of 1*H*- and 2*H*-1,2,3-triazole vibrationally excited states alongside provisional and practical computational predictions of the excited-state quartic centrifugal distortion constants. The low-energy fundamental vibrational states of 1*H*-1,2,3-triazole and five of its deuteriated isotopologues ([1-^{2}H]-, [4-^{2}H]-, [5-^{2}H]-, [4,5-^{2}H]-, and [1,4,5-^{2}H]-1*H*-1,2,3-triazole), as well as those of 2*H*-1,2,3-triazole and five of its deuteriated isotopologues ([2-^{2}H]-, [4-^{2}H]-, [2,4-^{2}H]-, [4,5-^{2}H]-, and [2,4,5-^{2}H]-2*H*-1,2,3-triazole), are studied using millimeter-wave spectroscopy in the 130–375 GHz frequency region. The normal and [2-^{2}H]-isotopologues of 2*H*-1,2,3-triazole are also analyzed using high-resolution infrared spectroscopy, determining the precise energies of three of their low-energy fundamental states. The resulting spectroscopic constants for each of the vibrationally excited states are reported for the first time. Coupled-cluster vibration–rotation interaction constants are compared with each of their experimentally determined values, often showing agreement within 500 kHz. Newly available coupled-cluster predictions of the excited-state quartic centrifugal distortion constants based on fourth-order vibrational perturbation theory are benchmarked using a large number of the 1,2,3-triazole tautomer isotopologues and vibrationally excited states studied.

INTRODUCTION

High-resolution infrared, microwave, and millimeter-wave spectroscopies enable the accurate and precise determination of molecular spectroscopic constants. While centrifugal distortion constants can sometimes be neglected in microwave studies (low values of J and K), they become necessary for the accurate modeling of most spectra involving transitions at the higher values of J and K that are typical in high-resolution infrared (IR) or millimeter-wave spectroscopy. As a result, accurate centrifugal distortion constants are critical for molecular identification in the interstellar medium (ISM) and other harsh environments.[1–3] Centrifugal distortion constants are dependent on the masses comprising the molecule and their locations, as well as on the molecular potential energy surfaces.[4] These constants are not simply empirical corrections to the rigid-rotor approximation used to accurately predict rotational transition frequencies; rather, they are physically meaningful terms that provide information about the mass distribution in a molecule and the vibrational motions of the atoms. Several decades ago, Watson provided reduced centrifugal distortion constants that are typically determined experimentally and predicted computationally.[5,6] Precise and accurate prediction of centrifugal

distortion constants has become common within the spectroscopy community for ground-state species.

All of the spectroscopic constants (rotational and centrifugal distortion) change for vibrationally excited states, relative to the ground state, as the mass distribution changes upon vibration. The vibration–rotation interaction constants, or "α values," which are the changes to the rotational constants from the ground-state values upon vibration, were described by Mills.[7] Analogously, the vibration–rotation interaction centrifugal distortion constants, or "β values," are the changes between the ground-state and vibrationally excited-state centrifugal distortion constants. Computational software has applied vibrational perturbation theory to predict rotational constants, centrifugal distortion constants up to sextic terms for the ground state, and vibration–rotation interaction (α) constants for vibrationally excited states. While numerous studies have determined centrifugal distortion constants for vibrationally excited states, their prediction is challenging and has not yet been implemented in any readily available computational chemistry software package. Computational predictions of the α and β terms are important, as vibrationally excited-state spectra are commonly obtained along with their ground-state spectra, particularly in millimeter-wave spectroscopy. Accurate predictions of these constants may assist in assigning the spectra of vibrationally excited states and the least-squares fitting where the centrifugal distortion constants are necessary to model the spectra but cannot be determined directly, e.g., Coriolis-coupled vibrationally excited states.[8–18] It is common practice in these cases to hold the vibrationally excited-state centrifugal distortion values at the corresponding ground-state values. There is a need for high-precision determination of the vibrationally excited-state centrifugal distortion constants and simultaneous determination of their computed values to provide important benchmarks.

Theoretical predictions for vibrationally excited-state quartic distortion constants have been sought for some time. Early efforts frequently targeted formulas specialized for certain atomic connectivities (D_{3h} triatomic, to name one example).[19] The fact that there exist many specialized formulas, most of which are highly algebraically complicated, has impeded their adoption and implementation into popular software packages. Aliev published a general formula for linear polyatomic molecules in 1986. It seems, however, to have gone largely unappreciated.[20] Numerical implementations based on contact transformation theory have recently proven successful. In 2004, the A-reduced rovibrational constants of water were predicted fully to the sixth order by Seghir and co-workers.[21] This comprises the equilibrium octic constants, the first vibrational correction to the sextics, up to second vibrational correction to the quartics, and up to the third vibrational correction to the rotational constants. At the time, their implementation was restricted to triatomic molecules. Watson discussed the vibrational dependence of the quartics in 2005.[22] He presented an expression in terms of rotational operators and commutators and made applications to a handful of nonlinear triatomics. Demaison, Margulès, and Boggs predicted the vibrational dependence for NH_2 using the VIBROT code[23] and similar calculations have been performed for SO_2.[24] A recent review included examples of higher-order perturbation theory applied to molecules as large as pentatomics.[25]

1*H*- and 2*H*-1,2,3-Triazoles ($C_2H_3N_3$, C_s, and C_{2v}, respectively), the subject of a recent semi-experimental equilibrium (r_e^{SE}) structure determination[26] and this work, are near-oblate asymmetric rotors as shown in Fig. 1. Although the equilibrium population of the 1*H* tautomer in the gas phase at room temperature is very small (ΔE = 4.2 kcal/mol; $K_{eq} \sim 10^{-3}$), the low population of the C_s tautomer (1*H*) is compensated by the fact that it is significantly more polar (μ = 4.24 D) than the C_{2v} tautomer (2*H*) (μ = 0.10 D). Consequently, the rotational spectra of both species are readily observable.[27–31] The rotational[26,32–35] and vibrational[36–39] spectra have been studied for the normal 1,2,3-triazole isotopologues, as well as several of their deuteriated counterparts.[32–34,37,38]

We previously analyzed the rotational spectra of many isotopologues of 1*H*- and 2*H*-1,2,3-triazole in order to determine a highly precise semi-experimental equilibrium structure for each molecule.[26] As is typical of such millimeter-wave studies, we also observed the rotational spectra of vibrationally excited states for a number of the isotopologues. In the current study, we report the assignment and analysis of these vibrationally excited states. These studies are augmented, significantly, by incorporation of additional experimental data obtained by high-resolution infrared spectroscopy and by theoretical predictions derived from new computational algorithms for evaluating centrifugal distortion constants for vibrationally excited states. Analyses of vibrationally excited states of multiple isotopologues have previously been performed,[15,17,18,40–48] often in the context of halogen isotopologues and usually involving fewer isotopologues than in the present work. The current study enables a more comprehensive comparison between the changes to spectroscopic constants upon vibrational excitation for several isotopologues. More importantly, it provides the opportunity to apply a practical and diagnostically useful computational

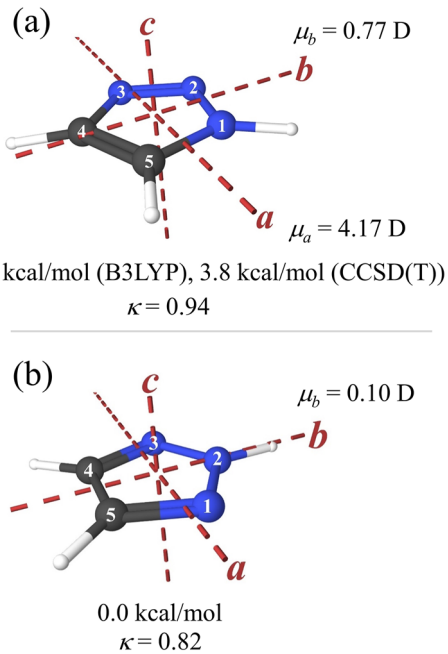

FIG. 1. (a) 1*H*-1,2,3-triazole and (b) 2*H*-1,2,3-triazole with principal inertial axes, dipole components [CCSD(T)/cc-pCVTZ], relative energies [B3LYP + ZPVE and CCSD(T)/cc-pCVTZ + ZPVE], and asymmetry parameters κ.

prediction of vibrationally excited-state centrifugal distortion constants to a somewhat complex molecule. High-resolution infrared spectra for 2*H*-1,2,3-triazole and [2-^{2}H]-2*H*-1,2,3-triazole provide the precise determination of vibrational state energies for their low-lying fundamental states.

EXPERIMENTAL METHODS

As a neat liquid, 1,2,3-triazole exists predominantly as the 1*H* tautomer by virtue of the effects of polarity/solvation. 1*H*-1,2,3-Triazole was obtained from Sigma-Aldrich or Oakwood Chemical. The sample obtained from Sigma-Aldrich was pink and that from Oakwood was colorless. The material from the first commercial source contained pyridazine as a major impurity, identified by the previously determined rotational spectrum,[49] and pyrazole, identified using its rotational constants.[50–52] In order to observe low-abundance isotopologues, the sample was purified by Kugelrohr distillation. Triazole from the second commercial source was of higher purity and was used without further purification. Deuteriated samples for millimeter-wave spectra were prepared through three synthetic routes.[26] The high-resolution IR spectrum of [2-^{2}H]-2*H*-1,2,3-triazole was obtained coincidentally while collecting the spectrum of the normal isotopologue, presumably due to hydrogen-deuterium exchange with deuteriated molecules that remained in the chamber from D_2O used in the preceding experiment.

Continuous broadband spectra in the 130–230 GHz and 235–375 GHz ranges were collected using 5–30 mTorr sample pressures at room temperature. The instrument has been described previously.[41,49,53] The spectrum from 130 to 375 GHz was obtained over approximately six days using the following experimental parameters: 0.045 kHz frequency increment, 0.6 MHz/s sweep rate, 10 ms time constant, and 50 kHz AM and 500 kHz FM modulation in a tone-burst design. Data for a given sample in these frequency ranges were combined into a single spectral file using Assignment and Analysis of Broadband Spectra (AABS) software.[54,55] In our least-squares fits, we assume a uniform 50 kHz frequency measurement uncertainty for all millimeter-wave transitions, including those from Stiefvater *et al.*[35]

High-resolution infrared data presented in this work were recorded at the Canadian Light Source (CLS) Synchrotron Far-IR beamline (February 2022) using a Bruker IFS 125 HR Spectrometer, with synchrotron radiation and a 9.4 m optical pathlength difference providing a nominal resolution of 0.000 96 cm^{-1}. The aperture was 1.15 mm, using a KBr beamsplitter, KBr cell windows, and a Ge:Cu detector, housed in a QMC cryogen-free cryostat (cooled by a Cryomech pulsed-tube cooler). The gain was set to 6×. The cell is a 2 m, White-type multi-pass cell; the total pathlength is 72 m. These spectra were obtained from 400 to 1200 cm^{-1} at a series of pressures for analysis of various vibrational states, which have substantially different infrared intensities. A uniform frequency measurement uncertainty of 0.000 18 cm^{-1} (~6 MHz) was assumed for all infrared measurements.

Software from the AABS suite was used for spectral combination and analysis.[54,55] Data were least-squares fit using ASFIT and ASROT,[56] as well as SPFIT and SPCAT.[57] AC and PIFORM programs were used for data formatting and presentation.[58,59] All least-squares fit files are provided in the supplementary material.

COMPUTATIONAL METHODS

To facilitate the preliminary analysis of experimental spectroscopic data, geometry optimizations with subsequent anharmonic frequency calculations using an ultrafine grid (*int* = *Grid* = *ultrafine*) were completed using Gaussian 16[60] at the B3LYP/6-311+G(2d,p) level of theory for the isotopologues of interest, providing predicted energies for the fundamental states, as well as vibration–rotation interaction terms. Computed relative energies are inclusive of zero-point vibrational energy (ZPVE) contributions. Computational output files are provided in the supplementary material.

Detailed computational and theoretical studies of the tautomers of 1,2,3-triazole were performed using the CCSD(T) method: coupled-cluster theory with a full, iterative treatment of single and double excitations and a perturbative estimate for triple excitations.[61–64] Relative energies including ZPVE contributions were computed at the CCSD(T)/cc-pCVTZ level of theory, as were vibrationally averaged dipole moments with anharmonic corrections. Quartic force fields, excluding the *ijkl* type constants, were obtained for all isotopologues by numerical differentiation of analytical gradients as implemented in the CFOUR program (Coupled-Cluster techniques for Computational Chemistry).[65,66] The ANO1 basis set was used, and the frozen-core approximation was made.[67] Additionally, optimizations and harmonic frequency computations were carried out with the cc-pwCVQZ basis set with all electrons correlated.[68–70] The harmonic frequencies and rotational constants in the CCSD(T)/ANO1 quartic force fields were replaced with the corresponding CCSD(T)/cc-pwCVQZ values.[71,72]

Rovibrational constants were predicted using a Vibrational Perturbation Theory (VPT) code written in Mathematica.[73] Anharmonic vibrational frequencies were evaluated with second-order vibrational perturbation theory (VPT2)—in some cases, treating Fermi resonances with the perturb-then-diagonalize schemes: VPT2+F or VPT2+K.[74,75] Fermi resonance interactions were treated explicitly if they displayed a variational-perturbational difference of greater than 1 cm^{-1}. The equilibrium sextic centrifugal distortion constants and vibrational corrections to the rotational constants were evaluated in the conventional way, from fourth-order vibrational perturbation theory (VPT4) and VPT2, respectively.[7,76–78] For the quartic centrifugal distortion constants, both the equilibrium values (from VPT2) and the first vibrational corrections (from VPT4) were evaluated. These fourth-order quartic distortion constants were obtained from an analytical implementation of a partially incomplete theory. Specifically, only the perturbation products proportional to J^4 were considered, neglecting perturbation products with higher powers of J capable of being reduced to J^4 through rotational angular momentum commutators.[77] In the notation used by Aliev and Watson, where the indices correspond to the number of vibrational and rotational operators, respectively, the following nine perturbation products were considered: $H_{32} \times H_{12}$, $H_{22} \times H_{22}$, $H_{22} \times H_{12} \times H_{30}$, $H_{12} \times H_{12} \times H_{40}$, $H_{22} \times H_{21} \times H_{21}$, $H_{12} \times H_{31} \times H_{21}$, $H_{12} \times H_{12} \times H_{30} \times H_{30}$, $H_{12} \times H_{21} \times H_{21} \times H_{30}$, and $H_{21} \times H_{21} \times H_{21} \times H_{21}$.[22,77] The full fourth-order expression and a thorough benchmark against experimental quartic constants will be presented in a later work. Although it is not obvious that the incomplete fourth-order treatment should be successful, preliminary comparisons have shown it to provide a reliable improvement over VPT2 for most molecules.

Its performance is less satisfactory for small, light molecules like H_2O and H_2CO.

ANALYSIS OF 1*H*-1,2,3-TRIAZOLE ROTATIONAL SPECTRA

Both 1*H*- and 2*H*-1,2,3-triazole exhibit a typical oblate-top band structure in our frequency region. The most intense peaks are sets of degenerate R-branch transitions in the $K_a = 0^+$ and 1^- series. The J values of the R-branch transitions decrease moving away from the bandhead and K_a values correspondingly increase. Eventually, these sets of transitions lose degeneracy, forming doublets of ${}^aR_{0,1}$ transitions (in the case of C_{2v} isotopologues) or quartets (of ${}^aR_{0,1}$, ${}^bR_{1,-1}$, and ${}^bR_{1,1}$ transitions in the case of C_s isotopologues). A small segment of the rotational spectrum, showing bandheads of each of the 1,2,3-triazole ground vibrational states of the normal isotopologues and the more widely spread bands of their much lower-intensity vibrational satellites, is presented in Fig. 2.

Transitions belonging to the four lowest-energy vibrationally excited states of 1*H*-1,2,3-triazole were observed: fundamentals ν_{18}, ν_{17}, ν_{16}, and ν_{15}. The vibrational manifolds up to 900 cm^{-1} for 1*H*- and 2*H*-1,2,3-triazole isotopologues described in this work are plotted in Figs. 3 and 4, respectively. For 1*H*-1,2,3-triazole, the lowest-energy vibrationally excited state, ν_{18} (561 cm^{-1}, A″), mainly

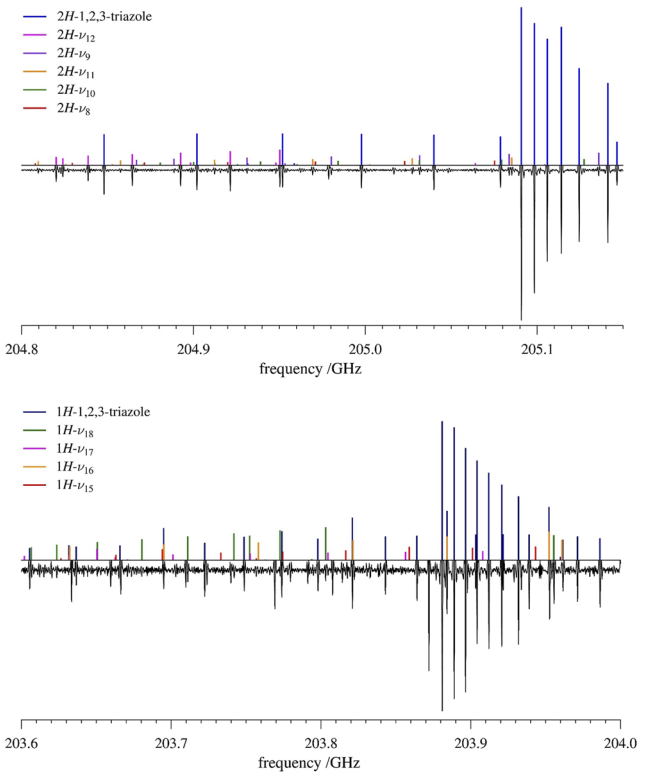

FIG. 2. Predicted stick and experimental spectra from 204.80 to 205.15 GHz displaying 2*H*-1,2,3-triazole (top) and from 203.6 to 204.0 GHz displaying 1*H*-1,2,3-triazole (bottom) of the normal isotopologues and their vibrationally excited states. Transitions belonging to each tautomer are visible in both spectra but are only labeled in the one in which they dominate.

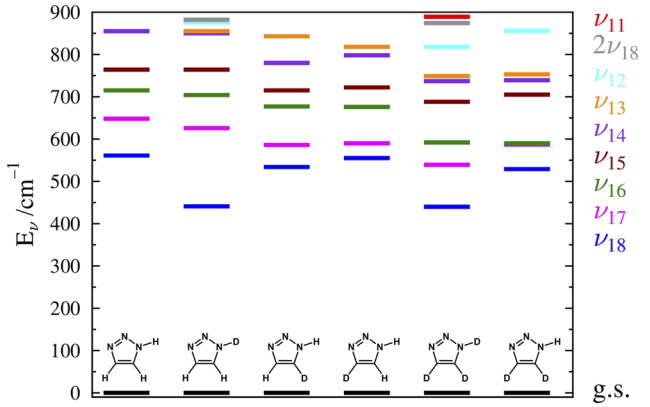

FIG. 3. Vibrational energy levels of 1*H*-1,2,3-triazole isotopologues, below 900 cm^{-1}. Fundamental frequencies were predicted with VPT2 based on the CCSD(T) quartic force fields described in the Computational Methods section. Labels on the right-hand side correspond in color and relative order along the *y*-axis to the vibrational states represented in that color.

comprises the out-of-plane N–H bend. The second fundamental, ν_{17} (648 cm^{-1}, A″), involves a torsion of the C–C bond relative to the N-atoms, with an out-of-plane N–H bend. The third fundamental, ν_{16} (715 cm^{-1}, A″), is the N2–N3 torsion relative to the rest of the ring. The motion associated with ν_{15} (764 cm^{-1}, A″) is a symmetric, out-of-plane wag of the C–H bonds. Fortuitously, the observed vibrational states of the main isotopologue are sufficiently distant in energy that no perturbation due to Coriolis-coupling is apparent in the observed transitions. As expected, the frequency of the lowest-energy vibrationally excited state decreases when hydrogen is substituted with deuterium, easily observed in Fig. 3 for ν_{18}. Deuteriation of triazole results in several of the vibrationally excited states moving closer together in energy. Thus, it is expected that couplings will arise for some vibrational states of the [1-^{2}H]-, [4-^{2}H]-, [5-^{2}H]-, and [4,5-^{2}H]-1*H*-1,2,3-triazole isotopologues that were not observed for their normal-isotopologue counterparts.

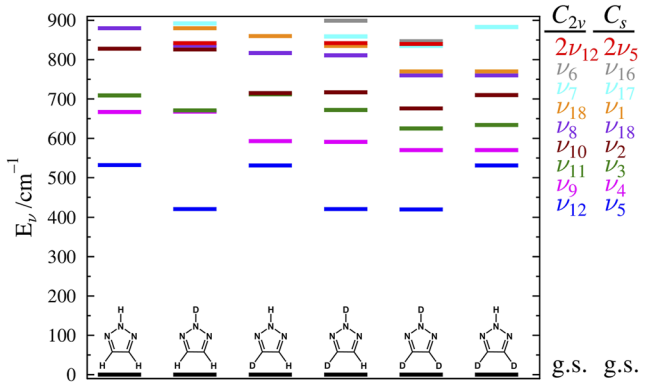

FIG. 4. Vibrational energy levels of 2*H*-1,2,3-triazole isotopologues, below 900 cm^{-1}. Fundamental frequencies were predicted with VPT2 based on the CCSD(T) quartic force fields described in the Computational Methods section. Due to certain substitution patterns changing the molecular symmetry from C_{2v} to C_s, state labels change for the two symmetries and are provided on the right. Matching colors indicate analogous vibrational motions.

For the normal isotopologue of 2*H*-1,2,3-triazole, we observed transitions for five vibrationally excited states: ν_{12} (532 cm^{-1}, B_1), the out-of-plane N–H wag; ν_9 (667 cm^{-1}, A_2), the C–C bond torsion relative to the N-atoms; ν_{11} (709 cm^{-1}, B_1), the symmetric, out-of-plane bend of the N–N–C bonds; ν_{10} (828 cm^{-1}, B_1), the symmetric, out-of-plane wag of the C–H bonds; and ν_8 (880 cm^{-1}, A_2), an antisymmetric, out-of-plane C–H bond wag. Similar to the 1*H*-tautomer, deuterium substitution at the nitrogen atom results in a substantial decrease in the frequency of the lowest-energy vibrationally excited state.

TABLE I. Experimental and computational spectroscopic constants for vibrational states of the normal isotopologue of 1*H*-1,2,3-triazole (S-reduced Hamiltonian, III^r representation).

	Ground state		ν_{18} (A″, 561 cm^{-1})[a]		ν_{17} (A″, 648 cm^{-1})[a]	
	CCSD(T)[b]	Experimental	CCSD(T)[c]	Experimental	CCSD(T)[c]	Experimental
A_v (MHz)	10 031.6	10 030.800 91 (26)	10 011.0995	10 011.209 (16)	10 001.7569	10 001.253 (30)
B_v (MHz)	9 869.6	9 870.690 16 (27)	9 846.5670	9 846.181 (16)	9 847.1537	9 846.256 (31)
C_v (MHz)	4 972.3	4 972.941 28 (21)	4 971.7822	4 971.518 12 (27)	4 974.2858	4 974.330 00 (81)
D_J (kHz)	3.65	3.683 91 (31)	3.68	3.686 54 (29)	3.64	3.637 2 (30)
D_{JK} (kHz)	−5.72	−5.772 36 (19)	−5.76	−5.754 91 (35)	−5.66	−5.602 5 (66)
D_K (kHz)	2.46	2.490 22 (25)	2.48	2.473 64 (27)	2.42	2.367 4 (35)
d_1 (kHz)	0.035 7	0.039 01 (35)	0.0404	[0.040 4]	0.0424	[0.042 4]
d_2 (kHz)	0.017 6	0.016 043 (77)	0.0179	[0.017 9]	0.0123	[0.012 3]
H_J (Hz)	0.001 46	0.000 78 (15)		[0.000 78]		[0.000 78]
H_{JK} (Hz)	−0.006 22	−0.006 045 (54)		[−0.006 045]		[−0.006 045]
H_{KJ} (Hz)	0.008 07	0.007 95 (13)		[0.007 95]		[0.007 95]
H_K (Hz)	−0.003 30	−0.002 96 (15)		[−0.002 96]		[−0.002 96]
h_1 (Hz)	0.000 167	[0.000 167]		[0.000 167]		[0.000 167]
h_2 (Hz)	−0.000 283	[−0.000 283]		[−0.000 283]		[−0.000 283]
h_3 (Hz)	0.000 135	[0.000 135]		[0.000 135]		[0.000 135]
N_{lines}[d]		838[e]		228		103
σ (MHz)		0.033		0.045		0.045

	ν_{16} (A″, 715 cm^{-1})[a]		ν_{15} (A″, 764 cm^{-1})[a]	
	CCSD(T)[c]	Experimental	CCSD(T)[c]	Experimental
A_v (MHz)	10 003.0140	10 003.17 (10)	10 003.6294	10 004.07 (27)
B_v (MHz)	9 833.2139	9 831.58 (10)	9 856.7590	9 855.81 (26)
C_v (MHz)	4 973.7949	4 973.889 19 (91)	4 975.1131	4 975.071 9 (12)
D_J (kHz)	3.61	3.623 0 (40)	3.59	3.595 3 (54)
D_{JK} (kHz)	−5.58	−5.523 7 (87)	−5.58	−5.539 (12)
D_K (kHz)	2.38	2.303 4 (47)	2.39	2.344 9 (64)
d_1 (kHz)	0.0299	[0.029 9]	0.0712	[0.071 2]
d_2 (kHz)	0.0112	[0.011 2]	0.0188	[0.018 8]
H_J (Hz)		[0.000 78]		[0.000 78]
H_{JK} (Hz)		[−0.006 045]		[−0.006 045]
H_{KJ} (Hz)		[0.007 95]		[0.007 95]
H_K (Hz)		[−0.002 96]		[−0.002 96]
h_1 (Hz)		[0.000 167]		[0.000 167]
h_2 (Hz)		[−0.000 283]		[−0.000 283]
h_3 (Hz)		[0.000 135]		[0.000 135]
N_{lines}[d]		88		63
σ (MHz)		0.045		0.048

[a]Fundamental frequencies were predicted with VPT2 based on the CCSD(T) quartic force fields described in the Computational Methods section.
[b]Calculated with provisional treatment described in "Computational Methods."
[c]Experimentally determined ground-state constants adjusted by the corresponding computed VPT2 α or VPT4 β values, based on the quartic force field.
[d]Number of independent transitions.
[e]Transitions reported by Stiefvater *et al.*[35] are included in the least-squares fit.

Although the spectroscopic constants for the ground vibrational state of all isotopologues discussed herein have been reported previously,[26] the values are slightly modified here by the incorporation of computed approximate VPT4 centrifugal distortion constants for those centrifugal distortion terms that could not be determined. The least-squares fitted parameters for the five lowest-energy vibrational states of the normal isotopologue of 1*H*-1,2,3-triazole are provided in Table I, alongside the predicted constants for each observed state. Rotational and quartic centrifugal distortion constants for vibrationally excited states were predicted by calculating the change from computed ground-state value to computed excited-state value, i.e., $\alpha_x = B_0^x - B_v^x$ and $\beta_x = D_0^x - D_v^x$ values, respectively,

TABLE II. Experimental and computational spectroscopic constants for vibrational states of deuteriated isotopologues of 1*H*-1,2,3-triazole (S-reduced Hamiltonian, III^r representation).

	[1–^{2}H]-1*H*-1,2,3-triazole					
	Ground state		ν_{18} (A″, 441 cm^{-1})[a]		ν_{17} (A″, 626 cm^{-1})[a]	
	CCSD(T)[b]	Experimental	CCSD(T)[c]	Experimental	CCSD(T)[c]	Experimental
A_v (MHz)	9965.31	9967.792 48 (30)	9929.87	9929.592 (36)	9937.10	9937.66 (16)
B_v (MHz)	9162.58	9160.302 29 (25)	9158.30	9158.167 (32)	9136.57	9135.66 (12)
C_v (MHz)	4771.30	4771.761 34 (16)	4773.64	4773.581 51 (84)	4773.19	4773.165 8 (26)
D_J (kHz)	3.33	3.358 39 (14)	3.325	3.332 8 (36)	3.308	3.426 (22)
D_{JK} (kHz)	−5.18	−5.234 22 (22)	−5.163	−5.164 6 (79)	−5.106	−5.284 (45)
D_K (kHz)	2.21	2.239 29 (13)	2.20	2.197 3 (42)	2.16	2.218 (23)
d_1 (kHz)	−0.240	−0.242 59 (32)	−0.222	[−0.222]	−0.227	[−0.227]
d_2 (kHz)	0.009 0	0.010 13 (11)	0.0124	[0.012 4]	0.0189	[0.018 9]
H_J (Hz)	0.001 22	[0.001 22]		[0.001 22]		[0.001 22]
H_{JK} (Hz)	−0.005 19	[−0.005 19]		[−0.005 19]		[−0.005 19]
H_{KJ} (Hz)	0.006 76	[0.006 76]		[0.006 76]		[0.006 76]
H_K (Hz)	−0.002 79	[−0.002 79]		[−0.002 79]		[−0.002 79]
h_1 (Hz)	0.000 115	[0.000 115]		[0.000 115]		[0.000 115]
h_2 (Hz)	0.000 024 4	[0.000 024 4]		[0.000 024 4]		[0.000 024 4]
h_3 (Hz)	0.000 005 0	[0.000 005 0]		[0.000 005 0]		[0.000 005 0]
N_{lines}[d]		502		97		38
σ (MHz)		0.039		0.048		0.053

	[4-^{2}H]-1*H*-1,2,3-triazole				[5-^{2}H]-1*H*-1,2,3-triazole			
	Ground state		ν_{18} (A″, 555 cm^{-1})[a]		Ground state		ν_{18} (A″, 534 cm^{-1})[a]	
	CCSD(T)[b]	Experimental	CCSD(T)[c]	Experimental	CCSD(T)[b]	Experimental	CCSD(T)[c]	Experimental
A_v (MHz)	9885.91	9888.396 21 (62)	9854.15	[9854.1]	9994.58	9992.087 77 (66)	9950.03	9951.45 (37)
B_v (MHz)	9114.81	9113.048 56 (52)	9100.21	9100.048 (20)	9014.31	9016.982 98 (45)	9004.85	9003.49 (32)
C_v (MHz)	4739.93	4740.530 54 (17)	4740.25	4740.091 3 (26)	4737.18	4737.864 55 (17)	4739.50	4739.538 7 (23)
D_J (kHz)	3.30	3.329 73 (33)	3.340	3.350 (14)	3.26	3.284 98 (47)	3.238	3.233 (18)
D_{JK} (kHz)	−5.15	−5.199 04 (47)	−5.218	−5.220 (16)	−5.08	−5.132 49 (75)	−5.035	−5.019 (21)
D_K (kHz)	2.20	2.225 59 (33)	2.24	[2.24]	2.18	2.204 80 (45)	2.16	[2.16]
d_1 (kHz)	−0.275	−0.280 38 (71)	−0.290	[−0.290]	−0.107	−0.107 2 (11)	−0.0705	[−0.070 5]
d_2 (kHz)	−0.046 8	−0.045 8 (12)	−0.0534	[−0.053 4]	−0.041 5	−0.046 0 (19)	−0.0599	[−0.059 9]
H_J (Hz)	0.001 29	[0.001 29]		[0.001 29]	0.001 34	[0.001 3]		[0.001 3]
H_{JK} (Hz)	−0.005 36	[−0.005 36]		[−0.005 36]	−0.005 48	[−0.005 48]		[−0.005 48]
H_{KJ} (Hz)	0.006 90	[0.006 90]		[0.006 90]	0.006 95	[0.006 95]		[0.006 95]
H_K (Hz)	−0.002 83	[−0.002 83]		[−0.002 83]	−0.002 82	[−0.002 82]		[−0.002 82]
h_1 (Hz)	0.000 102	[0.000 102]		[0.000 102]	0.000 132	[0.000 132]		[0.000 132]
h_2 (Hz)	0.000 121	[0.000 121]		[0.000 121]	0.000 105	[0.000 105]		[0.000 105]
h_3 (Hz)	0.000 010 4	[0.000 010 4]		[0.000 010 4]	−0.000 003 4	[−0.000 003 4]		[−0.000 003 4]
N_{lines}[d]		392		21		358		28
σ (MHz)		0.036		0.052		0.037		0.046

TABLE II. (*Continued.*)

	[1,4,5-^{2}H]-1*H*-1,2,3-triazole				[4,5-^{2}H]-1*H*-1,2,3-triazole			
	Ground state		ν_{18} (A″, 440 cm^{-1})[a]		Ground state		ν_{18} (A″, 529 cm^{-1})[a]	
	CCSD(T)[b]	Experimental	CCSD(T)[c]	Experimental	CCSD(T)[b]	Experimental	CCSD(T)[c]	Experimental
A_v (MHz)	8943.37	8946.165 84 (36)	8914.99	8914.87 (13)	9195.43	9193.245 81 (19)	9158.85	9158.599 (22)
B_v (MHz)	8502.93	8500.444 16 (30)	8499.29	8498.99 (12)	8925.69	8928.273 11 (18)	8911.39	8911.468 (21)
C_v (MHz)	4356.92	4357.362 69 (19)	4358.97	4358.931 55 (71)	4527.07	4527.666 58 (11)	4528.99	4529.037 67 (31)
D_J (kHz)	2.68	2.706 82 (16)	2.685	2.683 0 (44)	2.94	2.962 352 (78)	2.938	2.946 46 (83)
D_{JK} (kHz)	−4.21	−4.252 07 (29)	−4.204	−4.191 1 (97)	−4.62	−4.663 491 (90)	−4.606	−4.560 3 (14)
D_K (kHz)	1.81	1.832 97 (15)	1.81	1.798 2 (55)	2.00	2.018 421 (75)	1.99	1.935 02 (100)
d_1 (kHz)	−0.165	−0.168 79 (28)	−0.155	[−0.155]	−0.003	−0.000 96 (14)	0.0316	[0.031 6]
d_2 (kHz)	−0.015 4	−0.014 98 (18)	−0.0134	[−0.013 4]	0.008 8	0.008 14 (14)	0.0255	[0.025 5]
H_J (Hz)	0.001 02	[0.001 02]		[0.001 02]	0.001 20	[0.001 20]		[0.001 20]
H_{JK} (Hz)	−0.004 14	[−0.004 14]		[−0.004 14]	−0.004 88	[−0.004 88]		[−0.004 88]
H_{KJ} (Hz)	0.005 23	0.005 056 (92)		0.005 056 (92)	0.006 15	[0.006 15]		[0.006 15]
H_K (Hz)	−0.002 11	[−0.002 11]		[−0.002 11]	−0.002 48	[−0.002 48]		[−0.002 48]
h_1 (Hz)	0.000 057	[0.000 057]		[0.000 057]	0.000 073	[0.000 073]		[0.000 073]
h_2 (Hz)	0.000 046	[0.000 046]		[0.000 046]	−0.000 072	[−0.000 072]		[−0.000 072]
h_3 (Hz)	0.000 011 6	[0.000 011 6]		[0.000 011 6]	0.000 018 7	[0.000 018 7]		[0.000 018 7]
N_{lines}[d]		543		62		718		94
σ (MHz)		0.039		0.047		0.036		0.040

[a]Fundamental frequencies were predicted with VPT2 based on the CCSD(T) quartic force fields described in the Computational Methods section.
[b]Calculated with provisional treatment described in "Computational Methods."
[c]Experimentally determined ground-state constants adjusted by the corresponding computed VPT2 α or VPT4 β values, based on the quartic force field.
[d]Number of independent transitions.

and applying this change to the experimentally determined ground-state value. All excited-state sextic centrifugal distortion constants that could not be determined were held constant at the corresponding ground-state value, as no computational values are available. While the dipole moment of 1*H*-1,2,3-triazole can compensate for its low population relative to 2*H*-1,2,3-triazole, allowing its rotational spectrum to be recorded in this work, the relative intensities of the infrared transitions are almost entirely dependent on the populations. Thus, 1*H*-1,2,3-triazole was not observed in the high-resolution infrared spectrum, and no vibrational energies were measured for its excited states. Rotational constants for the ground and excited vibrational states are predicted within 0.03% of their experimental values. For the ground state, where all quartic centrifugal distortion constants and several sextic constants could be determined, the purely computational values are in good agreement—all quartic terms are within 10% of their experimental values, and the three on-diagonal sextic terms other than H_J are within 12%. The experimental value of H_J is approximately one-half its predicted value. The experimentally determined value of H_J may be affected by the need to hold the off-diagonal terms constant at their predicted values and may not be reliable. The computational values of the quartic centrifugal distortion constants that could be determined for the vibrationally excited states are within 4% of their predicted values, which is quite good agreement. Importantly, there is nearly always better agreement between the computed values of the quartic centrifugal distortion constants with their experimental counterparts than the agreement between the ground- and excited-state centrifugal distortion constants.

Spectroscopic constants for [1-^{2}H]-, [4-^{2}H]-, [5-^{2}H]-, [1,4,5-^{2}H]-, and [4,5-^{2}H]-1*H*-1,2,3-triazole and their observed vibrationally excited states are provided in Table II. The predicted rotational constants are all within 0.1% of their experimental values. On-diagonal quartic distortion constants are within 4%, as are most of the off-diagonal quartic distortion constants. The only large discrepancy occurs for [4,5-^{2}H]-1*H*-1,2,3-triazole, whose ground-state experimental value of d_1 is nearly one-third its predicted value. The substantial error may be related to the quite small magnitudes of the computed and experimental constants, which are the smallest magnitude of any of the off-diagonal quartic distortion constants. The computed d_1 and d_2 values for ν_{18} of [4,5-^{2}H]-1*H*-1,2,3-triazole differ in both sign and order of magnitude from the computed and experimental ground-state values. Importantly, as with the normal isotopologue, there is consistently better agreement between the computed values of the quartic distortion constants with their experimental counterparts than with the ground-state values.

ANALYSIS OF 2*H*-1,2,3-TRIAZOLE ROTATIONAL AND INFRARED SPECTRA

In addition to data from the millimeter-wave spectrum, the high-resolution infrared spectrum of 2*H*-1,2,3-triazole was

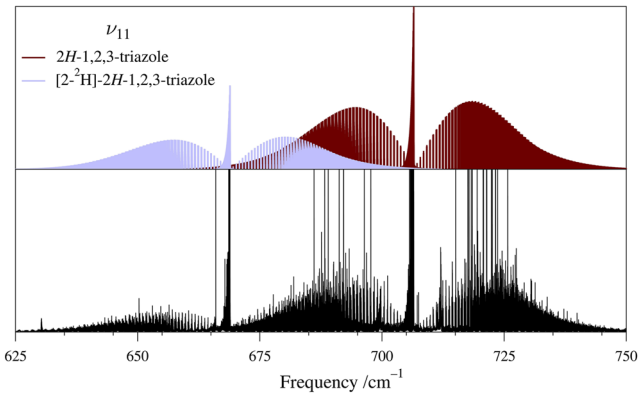

FIG. 5. Predicted stick spectrum from 625 to 750 cm^{-1} (top) experimental high-resolution infrared spectrum (bottom) of 2*H*-1,2,3-triazole and the unintentional but fortuitously observed [2-^{2}H]-2*H*-1,2,3-triazole.

measured, enabling the determination of several vibrational-state energies. Figure 5 displays a segment of the infrared spectrum, which includes the unintentional, but fortuitous and quite clear signals of the [2-^{2}H]-2*H*-1,2,3-triazole isotopologue. Spectroscopic constants for the vibrational states of the normal isotopologue are provided in Table III. Rotational and centrifugal distortion constants for the ground state are fitted using a single-state model with only millimeter-wave data. Since several sextic and, in some cases, quartic centrifugal distortion constants could not be determined experimentally for the vibrationally excited states and had to be held constant, they are held constant at the corresponding ground-state (sextic) or computed (quartic) values. When infrared transitions are included in the least-squares fit, however, the spectroscopic constants for the ground- and exited-states become dependent on one another. As a result, holding excited-state terms fixed at the ground-state value while fitting that ground-state value results in a mild distortion of the ground-state constant. In order to avoid such perturbation of the constants, in the combined-state least-squares fit, the ground-state values were held constant at the values determined from millimeter-wave spectra and excited-state constants were allowed to be fit—these constants are provided in Table III.

As in the case of 1*H*-1,2,3-triazole, the rotational constants for all of the observed vibrational states for the normal isotopologue of 2*H*-1,2,3-triazole are predicted within 0.1% of their experimental values. Most of the quartic centrifugal distortion constants are predicted within 7% of their experimental values. The exceptions are d_1 of ν_{10} (13%) and D_{JK} and D_K of ν_8 (13% and 35%, respectively). For the ground state, the predicted sextic distortion constants are within 40% (H_J), and the rest are within 11% of the values that could be determined. Overall, the spectroscopic constants are in good agreement between prediction and observation. While vibrationally excited-state sextic centrifugal distortion constants are yet beyond the capabilities of computational prediction, we have measured several such values for the first time for a few of the fundamental states of 2*H*-1,2,3-triazole. These values appear reasonably similar to those of the ground state, though ν_{10} displays some changes in its sextic terms by an order of magnitude. This may be physically meaningful or may be a result of the limited number of rotational transitions that were able to be observed and used for least-squares fitting.

Several infrared bands that, while less intense than the most intense bands of 2*H*-1,2,3-triazole, were nevertheless quite clear turned out to belong to [2-^{2}H]-2*H*-1,2,3-triazole. As previously mentioned, we attribute the abundance of this species to the fact that the experiment immediately preceding the triazole analysis involved deuterium oxide and an acid, which appear to have left a source of deuterium on the walls of the infrared cell. As a result, several vibrational energies of the [2-^{2}H]-2*H*-1,2,3-triazole have also been measured and are provided in Table IV alongside the spectroscopic constants. As with the normal isotopologue, the ground vibrational state was initially least-squares fit independently and then combined into the multi-state fit with its constants held fixed to the determined values.

The predicted rotational constants for [2-^{2}H]-2*H*-1,2,3-triazole, again, are within 0.1% of the experimentally determined values, and the quartic centrifugal distortion constants are within 13%, with one exception. The value of d_2 for ν_{11} (the third lowest-energy fundamental state) is nearly an order of magnitude smaller than predicted. Although it appears to be well-determined by the value of its uncertainty, it is determined using only high-resolution infrared data, as it was too low in intensity to be observed in the millimeter-wave spectrum. Given the lower precision of infrared data relative to millimeter-wave, there is a possibility that this term is less accurately determined than it appears. As shown in Fig. 4, upon deuteriation at the nitrogen atom, the energies of ν_{11} and ν_9 become quite close ($\Delta E_{11-9} \sim 3$ cm^{-1}) for [2-^{2}H]-2*H*-1,2,3-triazole. Since ν_9 has A_2 symmetry, its vibrational transitions have no infrared intensity. The rotational transitions of ν_{11} and ν_9 were too weak in the deuteriated samples studied to be measured. As a result, the Coriolis-coupling interaction cannot be properly addressed between ν_{11} and ν_9, providing additional uncertainty into the physical meaning of the ν_{11} spectroscopic constants. The sextic centrifugal distortion constants of the ground state are very well predicted—within 14% of the experimental values.

Other deuteriated isotopologues of 2*H*-1,2,3-triazole were, unsurprisingly, not in sufficiently high abundance to be observed in the high-resolution infrared spectrum. The vibrationally excited states of several deuteriated isotopologues were, however, observed in our millimeter-wave data. The computed and resultant spectroscopic constants for [4-^{2}H]-, [2,4-^{2}H]-, [2,4,5-^{2}H]-, and [4,5-^{2}H]-2*H*-1,2,3-triazoles are provided in Table V. The agreement between predicted and experimentally determined rotational constants for the vibrational states of the additional deuteriated isotopologues is, as with the other 1,2,3-triazoles, spectacular—all are predicted within 0.1% of their experimental values. The on-diagonal quartic distortion constants are all predicted within 4% (many of which are predicted within 1%), and the off-diagonal quartic distortion constants are predicted within 41% of those values that could be determined experimentally. While this error may appear large, it is reasonable for the smaller magnitude of the constants and, in most cases, compares better than a comparison of the ground-state value to the excited-state value. This comparison illustrates the utility of the approximate VPT4 treatment of the quartic centrifugal distortion constants used here.

TABLE III. Experimental and computational spectroscopic constants for vibrational states of the normal isotopologue of 2*H*-1,2,3-triazole (S-reduced Hamiltonian, III^r representation).

	Ground state		ν_{12} (B_1, 532 cm^{-1})[a]		ν_9 (A_2, 667 cm^{-1})[a]	
	CCSD(T)[b]	Experimental[c]	CCSD(T)[d]	Experimental[e]	CCSD(T)[d]	Experimental[c]
A_v (MHz)	10 256.1	10 252.030 68 (14)	10 241.8765	10 241.685 86 (10)	10 229.0521	10 229.363 3 (62)
B_v (MHz)	9 772.5	9 776.988 57 (14)	9 740.7395	9 740.296 26 (10)	9 748.5285	9 747.746 3 (66)
C_v (MHz)	5 001.7	5 002.457 50 (15)	4 999.8248	4 999.479 007 (87)	5 004.2802	5 004.285 78 (26)
D_J (kHz)	3.622	3.653 29 (22)	3.66	3.657 919 (68)	3.62	3.616 2 (12)
D_{JK} (kHz)	−5.660	−5.716 93 (14)	−5.71	−5.705 40 (12)	−5.62	−5.577 0 (27)
D_K (kHz)	2.437	2.465 81 (16)	2.46	2.453 980 (86)	2.41	2.364 8 (15)
d_1 (kHz)	0.110	0.113 250 (78)	0.1203	0.119 414 (15)	0.1067	[0.106 7]
d_2 (kHz)	0.015 2	0.015 177 (84)	0.0128	0.013 664 (15)	0.0117	[0.011 7]
H_J (Hz)	0.001 52	0.001 09 (11)		0.001 097 (14)		[0.001 09]
H_{JK} (Hz)	−0.006 31	−0.006 068 (40)		−0.005 902 (41)		[−0.006 068]
H_{KJ} (Hz)	0.008 07	0.007 627 (96)		0.007 495 (73)		[0.007 627]
H_K (Hz)	−0.003 27	−0.002 96 (10)		−0.002 947 (51)		[−0.002 96]
h_1 (Hz)	0.000 000 746	[0.000 000 746]		[0.000 000 746]		[0.000 000 746]
h_2 (Hz)	−0.000 149	[−0.000 149]		[−0.000 149]		[−0.000 149]
h_3 (Hz)	0.000 015 5	[0.000 015 5]		[0.000 015 5]		[0.000 015 5]
Energy (MHz)			15 976 972.022 (59)			
Energy (cm^{-1})			532.934 421 6 (20)			
N_{lines}[f]		912 / 0		575 / 4658		134 / 0
σ (MHz)		0.023		0.032 / 2.06		0.036

	ν_{11} (B_1, 709 cm^{-1})[a]		ν_{10} (B_1, 828 cm^{-1})[a]		ν_8 (A_2, 880 cm^{-1})[a]	
	CCSD(T)[d]	Experimental[e]	CCSD(T)[d]	Experimental[e]	CCSD(T)[d]	Experimental[c]
A_v (MHz)	10 230.1401	10 228.662 81 (40)	10 223.3211	10 223.408 57 (87)	10 228.4077	10 221.67 (97)
B_v (MHz)	9 738.2337	9 738.433 64 (41)	9 756.3109	9 756.158 95 (89)	9 741.9996	9 749.40 (89)
C_v (MHz)	5 003.0315	5 003.124 29 (17)	5 004.0050	5 004.026 87 (34)	5 002.7639	5 002.809 75 (61)
D_J (kHz)	3.58	3.586 36 (19)	3.58	3.582 87 (69)	3.24	3.148 (19)
D_{JK} (kHz)	−5.53	−5.474 31 (43)	−5.57	−5.499 8 (15)	−4.83	−4.274 (40)
D_K (kHz)	2.36	2.292 15 (30)	2.38	2.319 61 (95)	1.99	1.525 (21)
d_1 (kHz)	0.0874	0.091 016 (50)	0.132	0.131 17 (13)	0.0507	[0.050 7]
d_2 (kHz)	0.0239	0.024 431 (20)	0.0405	0.035 949 (48)	−0.0582	[−0.058 2]
H_J (Hz)		0.000 783 (36)		0.001 60 (18)		[0.001 09]
H_{JK} (Hz)		−0.003 94 (10)		−0.021 88 (58)		[−0.006 068]
H_{KJ} (Hz)		0.005 866 (84)		0.034 19 (74)		[0.007 627]
H_K (Hz)		[−0.002 96]		−0.014 28 (38)		[−0.002 96]
h_1 (Hz)		[0.000 000 746]		[0.000 000 746]		[0.000 000 746]
h_2 (Hz)		[−0.000 149]		[−0.000 149]		[−0.000 149]
h_3 (Hz)		[0.000 015 5]		[0.000 015 5]		[0.000 015 5]
Energy (MHz)	21 180 769.551 (89)		24 751 679.31 (16)			
Energy (cm^{-1})	706.514 423 1 (30)		825.627 151 4 (53)			
N_{lines}[f]	135 / 4081		35 / 2170		35 / 0	
σ (MHz)	0.035 / 2.28		0.034 / 3.08		0.029	

[a]Fundamental frequencies were predicted with VPT2 based on the CCSD(T) quartic force fields described in the Computational Methods section.
[b]Calculated with provisional treatment described in "Computational Methods."
[c]Spectroscopic constants determined using millimeter-wave data only.
[d]Experimentally determined ground-state constants adjusted by the corresponding computed VPT2 α or VPT4 β values, based on the quartic force field.
[e]Spectroscopic constants determined using combination of millimeter-wave and infrared data.
[f]Number of independent transitions (millimeter-wave/infrared).

TABLE IV. Experimental and computational spectroscopic constants for vibrational states of [2-^{2}H]-2*H*-1,2,3-triazole (S-reduced Hamiltonian, III^r representation).[a]

	Ground state		ν_{12} (B_1, 421 cm^{-1})[b]	
	CCSD(T)[c]	Experimental[d]	CCSD(T)[e]	Experimental[f]
A_v (MHz)	9774.6	9778.795 92 (42)	9737.319 1	9737.308 31 (14)
B_v (MHz)	9469.7	9465.815 41 (50)	9467.400 4	9466.975 70 (12)
C_v (MHz)	4807.8	4808.309 19 (44)	4809.348 5	4809.247 691 (58)
D_J (kHz)	3.30	3.326 12 (51)	3.31	3.308 943 (28)
D_{JK} (kHz)	−5.14	−5.193 89 (45)	−5.15	−5.142 789 (72)
D_K (kHz)	2.21	2.230 36 (47)	2.21	2.199 759 (57)
d_1 (kHz)	−0.258	−0.262 65 (55)	−0.252	−0.251 910 (24)
d_2 (kHz)	0.003 78	0.003 601 (72)	0.003 60	0.004 138 (24)
H_J (Hz)	0.001 28	0.001 22 (25)		[0.001 22]
H_{JK} (Hz)	−0.005 29	−0.005 32 (10)		[−0.005 32]
H_{KJ} (Hz)	0.006 78	0.007 30 (23)		[0.007 30]
H_K (Hz)	−0.002 76	−0.003 20 (25)		[−0.003 20]
h_1 (Hz)	0.000 074 9	[0.000 074 9]		[0.000 074 9]
h_2 (Hz)	−0.000 096 9	[−0.000 096 9]		[−0.000 096 9]
h_3 (Hz)	−0.000 021 3	[−0.000 021 3]		[−0.000 021 3]
Energy (MHz)				12 620 338.315 (86)
Energy (cm^{-1})				420.969 173 1 (29)
N_{lines}[g]		478 / 0		203 / 2487
σ (MHz)		0.036		0.039 / 2.09
	ν_{11} (B_1, 671 cm^{-1})		ν_{10} (B_1, 826 cm^{-1})	
	CCSD(T)[e]	Experimental[h]	CCSD(T)[e]	Experimental[h]
A_v (MHz)	9739.3060	9 739.265 95 (96)	9757.3455	9757.314 7 (16)
B_v (MHz)	9443.2819	9 442.844 81 (92)	9441.4724	9441.227 9 (15)
C_v (MHz)	4809.1186	4 809.107 93 (29)	4809.6376	4809.690 4 (11)
D_J (kHz)	3.24	3.246 77 (17)	3.25	3.254 51 (45)
D_{JK} (kHz)	−4.98	−4.922 93 (39)	−5.03	−4.789 9 (12)
D_K (kHz)	2.11	2.039 67 (25)	2.14	1.933 8 (11)
d_1 (kHz)	−0.222	−0.213 00 (27)	−0.263	−0.267 77 (53)
d_2 (kHz)	0.0135	0.002 78 (14)	0.0234	0.025 10 (17)
H_J (Hz)		[0.001 22]		[0.001 22]
H_{JK} (Hz)		[−0.005 32]		[−0.005 32]
H_{KJ} (Hz)		[0.007 30]		[0.007 30]
H_K (Hz)		[−0.003 20]		[−0.003 20]
h_1 (Hz)		[0.000 074 9]		[0.000 074 9]
h_2 (Hz)		[−0.000 096 9]		[−0.000 096 9]
h_3 (Hz)		[−0.000 021 3]		[−0.000 021 3]
Energy (MHz)		20 053 382.10 (15)		24 676 720.40 (21)
Energy (cm^{-1})		668.908 825 9 (50)		823.126 791 3 (70)
N_{lines}[g]		0 / 2195		0 / 1241
σ (MHz)		0 / 2.43		0 / 3.39

[a]The second fundamental, ν_9 (A_2, 668 cm^{-1}), was too low in intensity in the millimeter-wave spectrum to be analyzed, and it is not IR-active.
[b]Fundamental frequencies were predicted with VPT2 based on the CCSD(T) quartic force fields described in the Computational Methods section.
[c]Calculated with provisional treatment described in "Computational Methods."
[d]Spectroscopic constants determined using millimeter-wave data only.
[e]Experimentally determined ground-state constants adjusted by the corresponding computed VPT2 α or VPT4 β values, based on the quartic force field.
[f]Spectroscopic constants determined using combination of millimeter-wave and infrared data.
[g]Number of independent transitions (millimeter-wave/infrared).
[h]Spectroscopic constants determined using infrared data only.

TABLE V. Experimental and computational spectroscopic constants for vibrational states of deuteriated isotopologues of 2*H*-1,2,3-triazole (S-reduced Hamiltonian, III^r representation).

	[4-^{2}H]-2*H*-1,2,3-triazole							
	Ground state		ν_{18} (A″, 531 cm^{-1})[a]		ν_{17} (A″, 593 cm^{-1})[a]		ν_{16} (A″, 712 cm^{-1})[a]	
	CCSD(T)[b]	Experimental	CCSD(T)[c]	Experimental	CCSD(T)[c]	Experimental	CCSD(T)[c]	Experimental
A_v (MHz)	10 014.76	10 013.840 70 (18)	9992.72	9992.613 93 (54)	9963.08	9962.660 5 (59)	9991.09	[9991.09]
B_v (MHz)	9 105.37	9 106.920 68 (15)	9083.88	9083.604 48 (68)	9095.03	9095.317 1 (41)	9083.12	9073.637 (49)
C_v (MHz)	4 766.89	4 767.628 82 (15)	4765.21	4764.869 81 (42)	4769.90	4769.974 09 (65)	4768.96	4768.251 7 (23)
D_J (kHz)	3.26	3.290 48 (11)	3.298	3.294 95 (83)	3.105	3.105 3 (13)	3.519	3.525 (27)
D_{JK} (kHz)	−5.09	−5.136 70 (15)	−5.141	−5.129 67 (63)	−4.761	−4.683 3 (14)	−5.520	−5.542 (30)
D_K (kHz)	2.18	2.203 21 (34)	2.20	2.194 30 (59)	2.01	1.936 4 (19)	2.37	[2.37]
d_1 (kHz)	−0.145	−0.145 42 (12)	−0.147	−0.139 47 (81)	−0.039	−0.027 6 (12)	−0.068	[−0.068]
d_2 (kHz)	−0.011 2	−0.011 63 (15)	−0.0126	−0.009 4 (13)	−0.000 475	[−0.000 475]	0.0554	[0.055 4]
H_J (Hz)	0.001 35	[0.001 35]		[0.001 35]		[0.001 35]		[0.001 35]
H_{JK} (Hz)	−0.005 46	[−0.005 46]		[−0.005 46]		[−0.005 46]		[−0.005 46]
H_{KJ} (Hz)	0.006 91	[0.006 91]		[0.006 91]		[0.006 91]		[0.006 91]
H_K (Hz)	−0.002 80	−0.002 79 (15)		−0.002 79 (15)		−0.002 79 (15)		−0.002 79 (15)
h_1 (Hz)	0.000 176	[0.000 176]		[0.000 176]		[0.000 176]		[0.000 176]
h_2 (Hz)	0.000 110	[0.000 110]		[0.000 110]		[0.000 110]		[0.000 110]
h_3 (Hz)	−0.000 004 8	[−0.000 004 8]		[−0.000 004 8]		[−0.000 004 8]		[−0.000 004 8]
N_{lines}[d]		713		266		105		24
σ (MHz)		0.032		0.038		0.040		0.047

	[2,4-^{2}H]-2*H*-1,2,3-triazole			
	Ground state		ν_{18} (A″, 421 cm^{-1})[a]	
	CCSD(T)[b]	Experimental	CCSD(T)[c]	Experimental
A_v (MHz)	9678.03	9679.665 82 (47)	9649.91	9649.94 (12)
B_v (MHz)	8723.96	8722.545 55 (38)	8715.06	8714.535 (99)
C_v (MHz)	4586.20	4586.675 23 (15)	4587.63	4587.529 44 (61)
D_J (kHz)	2.98	3.000 51 (24)	2.985	2.995 0 (45)
D_{JK} (kHz)	−4.62	−4.666 64 (47)	−4.630	−4.644 (11)
D_K (kHz)	1.97	1.988 21 (28)	1.97	1.974 4 (62)
d_1 (kHz)	−0.275	−0.277 56 (44)	−0.272	[−0.272]
d_2 (kHz)	−0.009 0	−0.008 03 (54)	−0.0076	[−0.007 6]
H_J (Hz)	0.001 14	[0.001 14]		[0.001 14]
H_{JK} (Hz)	−0.004 57	[−0.004 57]		[−0.004 57]
H_{KJ} (Hz)	0.005 79	[0.005 79]		[0.005 79]
H_K (Hz)	−0.002 36	[−0.002 36]		[−0.002 36]
h_1 (Hz)	0.000 170	[0.000 170]		[0.000 170]
h_2 (Hz)	0.000 051	[0.000 051]		[0.000 051]
h_3 (Hz)	0.000 013 5	[0.000 013 5]		[0.000 013 5]
N_{lines}[d]		326		66
σ (MHz)		0.037		0.039

TABLE V. (*Continued.*)

	[2,4,5-^{2}H]-2*H*-1,2,3-triazole							
	Ground state		ν_{12} (B_1, 420 cm^{-1})[a]		ν_9 (A_2, 570 cm^{-1})[a]		ν_{11} (B_1, 625 cm^{-1})[a]	
	CCSD(T)[b]	Experimental	CCSD(T)[c]	Experimental	CCSD(T)[c]	Experimental	CCSD(T)[c]	Experimental
A_v (MHz)	9083.24	9086.707 81 (17)	9050.98	9050.911 (11)	9046.47	9046.96 (23)	9060.17	9060.67 (57)
B_v (MHz)	8485.27	8482.461 42 (14)	8483.60	8483.256 (11)	8465.07	8464.92 (20)	8459.63	8459.75 (54)
C_v (MHz)	4385.26	4385.777 99 (14)	4386.64	4386.557 45 (29)	4387.52	4387.579 57 (56)	4388.13	4388.186 6 (41)
D_J (kHz)	2.68	2.702 779 (76)	2.689	2.688 1 (47)	2.653	2.670 6 (52)	2.441	2.502 (18)
D_{JK} (kHz)	−4.19	−4.229 92 (11)	−4.197	−4.190 2 (61)	−4.118	−4.076 (12)	−3.682	−3.743 (20)
D_K (kHz)	1.79	1.814 28 (25)	1.80	1.792 0 (17)	1.75	1.693 2 (72)	1.53	[1.53]
d_1 (kHz)	−0.264	−0.268 804 (95)	−0.2605	−0.261 (29)	−0.208	[−0.208]	−0.279	[−0.279]
d_2 (kHz)	−0.0204	−0.020 424 (55)	−0.0197	[−0.019 7]	0.0306	[0.030 6]	−0.096	[−0.096]
H_J (Hz)	0.001 03	[0.001 03]		[0.001 03]		[0.001 03]		[0.001 03]
H_{JK} (Hz)	−0.004 07	[−0.004 07]		[−0.004 07]		[−0.004 07]		[−0.004 07]
H_{KJ} (Hz)	0.005 12	[0.005 12]		[0.005 12]		[0.005 12]		[0.005 12]
H_K (Hz)	−0.002 07	−0.001 919 (88)		[−0.001 919]		[−0.001 919]		[−0.001 919]
h_1 (Hz)	0.000 105	[0.000 105]		[0.000 105]		[0.000 105]		[0.000 105]
h_2 (Hz)	−0.000 022 9	[−0.000 022 9]		[−0.000 022 9]		[−0.000 022 9]		[−0.000 022 9]
h_3 (Hz)	−0.000 007 3	[−0.000 007 3]		[−0.000 007 3]		[−0.000 007 3]		[−0.000 007 3]
N_{lines}[d]		722		193		54		16
σ (MHz)		0.035		0.035		0.037		0.044

	[4,5-^{2}H]-2*H*-1,2,3-triazole					
	Ground state		ν_{12} (B_1, 531 cm^{-1})[a]		ν_9 (A_2, 570 cm^{-1})[a]	
	CCSD(T)[b]	Experimental	CCSD(T)[c]	Experimental	CCSD(T)[c]	Experimental
A_v (MHz)	9144.71	9141.879 7 (19)	9132.83	9132.786 27 (78)	9121.67	9121.171 (48)
B_v (MHz)	9081.55	9085.183 8 (19)	9053.43	9053.124 37 (71)	9044.95	9045.780 (48)
C_v (MHz)	4554.37	4555.057 24 (15)	4552.78	4552.459 50 (15)	4556.92	4556.980 76 (34)
D_J (kHz)	2.93	2.956 45 (11)	2.965	2.963 09 (25)	2.88	2.897 86 (78)
D_{JK} (kHz)	−4.61	−4.653 18 (18)	−4.663	−4.651 62 (32)	−4.49	−4.424 7 (13)
D_K (kHz)	1.99	2.013 62 (13)	2.02	2.008 53 (27)	1.92	1.845 7 (14)
d_1 (kHz)	0.151	0.153 53 (85)	0.1578	0.140 0 (19)	0.096	[0.096]
d_2 (kHz)	−0.009 6	−0.009 32 (73)	−0.0061	−0.008 26 (80)	0.0331	[0.033 1]
H_J (Hz)	0.001 22	[0.001 22]		[0.001 22]		[0.001 22]
H_{JK} (Hz)	−0.004 88	[−0.004 88]		[−0.004 88]		[−0.004 88]
H_{KJ} (Hz)	0.006 13	0.006 022 (73)		[0.006 022]		[0.006 022]
H_K (Hz)	−0.002 47	[−0.002 47]		[−0.002 47]		[−0.002 47]
h_1 (Hz)	−0.000 040	[−0.000 040]		[−0.000 040]		[−0.000 040]
h_2 (Hz)	−0.000 057	[−0.000 057]		[−0.000 057]		[−0.000 057]
h_3 (Hz)	0.000 003 6	[0.000 003 6]		[0.000 003 6]		[0.000 003 6]
N_{lines}[d]		632		327		119
σ (MHz)		0.033		0.037		0.046

TABLE V. (*Continued.*)

	[4,5-^{2}H]-2*H*-1,2,3-triazole			
	ν_{11} (B_1, 634 cm^{-1})[a]		ν_{10} (B_1, 710 cm^{-1})[a]	
	CCSD(T)[c]	Experimental	CCSD(T)[c]	Experimental
A_v (MHz)	9115.30	9115.28 (23)	9124.00	9123.16 (12)
B_v (MHz)	9064.76	9064.44 (23)	9050.32	9050.83 (12)
C_v (MHz)	4558.01	4558.050 68 (31)	4555.54	4555.628 1 (10)
D_J (kHz)	2.649	2.656 0 (19)	2.884	2.883 5 (35)
D_{JK} (kHz)	−4.019	−3.959 2 (30)	−4.480	−4.431 8 (26)
D_K (kHz)	1.69	1.621 6 (17)	1.91	1.870 9 (25)
d_1 (kHz)	0.183	[0.183]	0.120	[0.120]
d_2 (kHz)	−0.0893	[−0.089 3]	0.0013	[0.001 3]
H_J (Hz)		[0.001 22]		[0.001 22]
H_{JK} (Hz)		[−0.004 88]		[−0.004 88]
H_{KJ} (Hz)		[0.006 022]		[0.006 022]
H_K (Hz)		[−0.002 47]		[−0.002 47]
h_1 (Hz)		[−0.000 040]		[−0.000 040]
h_2 (Hz)		[−0.000 057]		[−0.000 057]
h_3 (Hz)		[0.000 003 6]		[0.000 003 6]
N_{lines}[d]		64		49
σ (MHz)		0.039		0.044

[a]Fundamental frequencies were predicted with VPT2 based on the CCSD(T) quartic force fields described in the Computational Methods section.
[b]Calculated with provisional treatment described in "Computational Methods."
[c]Experimentally determined ground-state constants adjusted by the corresponding computed VPT2 α or VPT4 β values, based on the quartic force field.
[d]Number of independent transitions.

TABLE VI. Experimental and computational vibration–rotation interaction terms for observed 1*H*-1,2,3-triazole isotopologues (S-reduced Hamiltonian, III^r representation).[a]

	1*H*-1,2,3-triazole											
	ν_{18}			ν_{17}			ν_{16}			ν_{15}		
	B3LYP	CCSD(T)	Expt.	B3LYP	CCSD(T)	Expt.	B3LYP	CCSD(T)	Expt.	B3LYP	CCSD(T)	Expt.
A_0-A_v (MHz)	19.64	19.70	19.59	29.28	29.04	29.55	27.66	27.79	27.63	25.07	27.17	26.73
B_0-B_v (MHz)	22.70	24.12	24.51	24.37	23.54	24.43	38.74	37.48	39.11	12.90	13.93	14.88
C_0-C_v (MHz)	1.05	1.16	1.42	−1.53	−1.34	−1.39	−1.05	−0.85	−0.95	−2.62	−2.17	−2.13
$D_{J,0}-D_{J,v}$ (kHz)		−0.0005	−0.0026		0.0419	0.0467		0.0723	0.0609		0.0930	0.0886
$D_{JK,0}-D_{JK,v}$ (kHz)		−0.0104	−0.0175		−0.1084	−0.1699		−0.1885	−0.2487		−0.1955	−0.2334
$D_{K,0}-D_{K,v}$ (kHz)		0.0074	0.0166		0.0653	0.1228		0.1149	0.1868		0.1014	0.1453

	[1–^{2}H]-1*H*-1,2,3-triazole						[4-^{2}H]-1*H*-1,2,3-triazole			[5-^{2}H]-1*H*-1,2,3-triazole		
	ν_{18}			ν_{17}			ν_{18}			ν_{18}		
	B3LYP	CCSD(T)	Expt.	B3LYP	CCSD(T)	Expt.	B3LYP	CCSD(T)	Expt.	B3LYP	CCSD(T)	Expt.
A_0-A_v (MHz)	37.81	37.92	38.20	31.11	30.69	30.13	32.1	34.2		37.1	42.1	40.6
B_0-B_v (MHz)	0.79	2.00	2.14	24.13	23.73	24.64	11.6	12.8	13.0	13.0	12.1	13.5
C_0-C_v (MHz)	−2.22	−1.87	−1.82	−1.49	−1.43	−1.40	0.5	0.3	0.4	−1.6	−1.6	−1.7
$D_{J,0}-D_{J,v}$ (kHz)		0.0333	0.0256		0.0502	−0.0676		−0.0103	−0.0203		0.0470	0.0520
$D_{JK,0}-D_{JK,v}$ (kHz)		−0.0716	−0.0696		−0.1280	0.0498		0.0191	0.0210		−0.0976	−0.1135
$D_{K,0}-D_{K,v}$ (kHz)		0.0354	0.0420		0.0764	0.0213		−0.0137			0.0464	

	[1,4,5-^{2}H]-1*H*-1,2,3-triazole			[4,5-^{2}H]-1*H*-1,2,3-triazole		
	ν_{18}			ν_{18}		
	B3LYP	CCSD(T)	Expt.	B3LYP	CCSD(T)	Expt.
A_0-A_v (MHz)	30.98	31.18	31.30	30.89	34.39	34.65
B_0-B_v (MHz)	0.16	1.16	1.45	16.73	16.89	16.81
C_0-C_v (MHz)	−1.90	−1.61	−1.57	−1.32	−1.32	−1.37
$D_{J,0}-D_{J,v}$ (kHz)		0.0218	0.0238		0.0242	0.0159
$D_{JK,0}-D_{JK,v}$ (kHz)		−0.0485	−0.0610		−0.0576	−0.1032
$D_{K,0}-D_{K,v}$ (kHz)		0.0245	0.0348		0.0304	0.0834

[a]No off-diagonal quartic centrifugal distortion terms could be determined for any of the 1*H*-1,2,3-triazoles' fundamental states, so they are excluded from the table.

TABLE VII. Experimental and computational vibration–rotation interaction terms for observed 2*H*-1,2,3-triazole isotopologues (S-reduced Hamiltonian, III^r representation).

	2*H*-1,2,3-triazole								
	ν_{12}			ν_9			ν_{11}		
	B3LYP	CCSD(T)	Expt.	B3LYP	CCSD(T)	Expt.	B3LYP	CCSD(T)	Expt.
A_0-A_v (MHz)	8.11	10.15	10.34	22.34	22.98	22.67	22.68	21.89	23.37
B_0-B_v (MHz)	37.10	36.25	36.69	29.19	28.46	29.24	38.68	38.75	38.55
C_0-C_v (MHz)	2.40	2.63	2.98	−1.92	−1.82	−1.83	−0.81	−0.57	−0.67
$D_{J,0}-D_{J,v}$ (kHz)		−0.0041	−0.0046		0.0352	0.0371		0.0740	0.0669
$D_{JK,0}-D_{JK,v}$ (kHz)		−0.0037	−0.0115		−0.0941	−0.1399		−0.1846	−0.2426
$D_{K,0}-D_{K,v}$ (kHz)		0.0041	0.0118		0.0575	0.1010		0.1094	0.1737
$d_{1,0}-d_{1,v}$ (kHz)		−0.0071	−0.0062		0.0065			0.0259	0.0222
$d_{2,0}-d_{2,v}$ (kHz)		0.0024	0.0015		0.0034			−0.0087	−0.0093

	2*H*-1,2,3-triazole						[2-^{2}H]-2*H*-1,2,3-triazole		
	ν_{10}			ν_8			ν_{12}		
	B3LYP	CCSD(T)	Expt.	B3LYP	CCSD(T)	Expt.	B3LYP	CCSD(T)	Expt.
A_0-A_v (MHz)	26.71	28.71	28.62	21.54	23.62	30.36	41.49	41.48	41.49
B_0-B_v (MHz)	19.57	20.68	20.83	30.23	34.99	27.59	−2.73	−1.58	−1.16
C_0-C_v (MHz)	−1.88	−1.55	−1.57	−0.66	−0.31	−0.35	−1.45	−1.04	−0.94
$D_{J,0}-D_{J,v}$ (kHz)		0.0686	0.0704		0.4119	0.5053		0.017 7	0.017 2
$D_{JK,0}-D_{JK,v}$ (kHz)		−0.1517	−0.2171		−0.8888	−1.4429		−0.042 4	−0.051 1
$D_{K,0}-D_{K,v}$ (kHz)		0.0820	0.1462		0.4756	0.9408		0.0216	0.030 6
$d_{1,0}-d_{1,v}$ (kHz)		−0.0192	−0.0179		0.0625			−0.010 5	−0.010 7
$d_{2,0}-d_{2,v}$ (kHz)		−0.0254	−0.0208		0.0734			−0.000 001 8	−0.000 537 0

	[2-^{2}H]-2*H*-1,2,3-triazole						[4-^{2}H]-2*H*-1,2,3-triazole		
	ν_{11}			ν_{10}			ν_{18}		
	B3LYP	CCSD(T)	Expt.	B3LYP	CCSD(T)	Expt.	B3LYP	CCSD(T)	Expt.
A_0-A_v (MHz)	40.10	39.49	39.53	20.14	21.45	21.48	20.51	21.12	21.23
B_0-B_v (MHz)	22.38	22.53	22.97	22.64	24.34	24.59	22.27	23.04	23.32
C_0-C_v (MHz)	−0.89	−0.81	−0.80	−1.65	−1.33	−1.38	2.23	2.41	2.76
$D_{J,0}-D_{J,v}$ (kHz)		0.0901	0.0793		0.0734	0.0716		−0.0072	−0.0045
$D_{JK,0}-D_{JK,v}$ (kHz)		−0.2146	−0.2710		−0.1637	−0.4040		0.0048	−0.0070
$D_{K,0}-D_{K,v}$ (kHz)		0.1232	0.1907		0.0893	0.2966		−0.0007	0.0089
$d_{1,0}-d_{1,v}$ (kHz)		−0.0403	−0.0497		0.0001	0.0051		0.0019	−0.0059
$d_{2,0}-d_{2,v}$ (kHz)		−0.0099	0.0008		−0.0198	−0.0215		0.0010	−0.0022

	[4-^{2}H]-2*H*-1,2,3-triazole						[2,4-^{2}H]-2*H*-1,2,3-triazole		
	ν_{17}			ν_{16}			ν_{18}		
	B3LYP	CCSD(T)	Expt.	B3LYP	CCSD(T)	Expt.	B3LYP	CCSD(T)	Expt.
A_0-A_v (MHz)	51.17	50.76	51.18	29.53	22.75		30.35	29.76	29.73
B_0-B_v (MHz)	9.99	11.89	11.60	27.86	23.80	33.28	5.98	7.49	8.01
C_0-C_v (MHz)	−2.52	−2.27	−2.35	−0.75	−1.33	−0.62	−1.34	−0.96	−0.85
$D_{J,0}-D_{J,v}$ (kHz)		0.1854	0.1852		−0.2285	−0.2345		0.0159	0.0055
$D_{JK,0}-D_{JK,v}$ (kHz)		−0.3753	−0.4534		0.3838	0.4053		−0.0370	−0.0226
$D_{K,0}-D_{K,v}$ (kHz)		0.1885	0.2668		−0.1634			0.0185	0.0138
$d_{1,0}-d_{1,v}$ (kHz)		−0.1065	−0.1178		−0.0778			−0.0058	
$d_{2,0}-d_{2,v}$ (kHz)		−0.0112			−0.0670			−0.0004	

TABLE VII. (*Continued.*)

	[2,4,5-^{2}H]-2*H*-1,2,3-triazole								
	ν_{12}			ν_9			ν_{11}		
	B3LYP	CCSD(T)	Expt.	B3LYP	CCSD(T)	Expt.	B3LYP	CCSD(T)	Expt.
A_0-A_v (MHz)	35.71	35.73	35.80	39.20	40.23	39.75	25.25	26.54	26.04
B_0-B_v (MHz)	−2.10	−1.14	−0.79	16.54	17.39	17.54	21.16	22.83	22.71
C_0-C_v (MHz)	−1.23	−0.86	−0.78	−1.90	−1.74	−1.80	−2.61	−2.35	−2.41
$D_{J,0}-D_{J,v}$ (kHz)		0.0140	0.0147		0.0501	0.0322		0.2620	0.2008
$D_{JK,0}-D_{JK,v}$ (kHz)		−0.0325	−0.0397		−0.1114	−0.1539		−0.5478	−0.4869
$D_{K,0}-D_{K,v}$ (kHz)		0.0162	0.0223		0.0604	0.1211		0.2843	
$d_{1,0}-d_{1,v}$ (kHz)		−0.0083	−0.0078		−0.0605			0.0105	
$d_{2,0}-d_{2,v}$ (kHz)		−0.0008			−0.0511			0.0756	

	[4,5-^{2}H]-2*H*-1,2,3-triazole											
	ν_{12}			ν_9			ν_{11}			ν_{10}		
	B3LYP	CCSD(T)	Expt.	B3LYP	CCSD(T)	Expt.	B3LYP	CCSD(T)	Expt.	B3LYP	CCSD(T)	Expt.
A_0-A_v (MHz)	7.23	9.05	9.09	19.23	20.21	20.71	24.79	26.58	26.60	18.39	17.88	18.72
B_0-B_v (MHz)	32.30	31.75	32.06	39.20	40.23	39.40	20.19	20.42	20.74	34.00	34.87	34.35
C_0-C_v (MHz)	2.09	2.28	2.60	−2.04	−1.87	−1.92	−3.20	−2.95	−2.99	−0.70	−0.48	−0.57
$D_{J,0}-D_{J,v}$ (kHz)		−0.0090	−0.0066		0.0724	0.0586		0.3076	0.3005		0.0725	0.0729
$D_{JK,0}-D_{JK,v}$ (kHz)		0.0099	−0.0016		−0.1681	−0.2285		−0.6345	−0.6940		−0.1731	−0.2214
$D_{K,0}-D_{K,v}$ (kHz)		−0.0034	0.0051		0.0946	0.1679		0.3254	0.3920		0.0998	0.1427
$d_{1,0}-d_{1,v}$ (kHz)		−0.0043	0.0135		0.0579			−0.0297			0.0336	
$d_{2,0}-d_{2,v}$ (kHz)		−0.0032	−0.0011		−0.0425			0.0800			−0.0107	

COMPARISON OF COMPUTED AND EXPERIMENTAL VIBRATION-ROTATION INTERACTION TERMS

Considering the sometimes rather small changes in the spectroscopic constants between ground and vibrationally excited states, it is worthwhile to examine the α and β values, directly, because the apparent agreement between the computed and experimental spectroscopic constants could be due simply to the relatively larger size of the constant compared with the change. Such comparisons for the B3LYP (α-only) and CCSD(T) methods are provided in Table VI for 1*H*-1,2,3-triazole isotopologues and in Table VII for 2*H*-1,2,3-triazole isotopologues. Both computational methods estimate the α values for the *A* and *B* rotational constants reasonably well—often within 10%. The CCSD(T) method, however, is almost always better than B3LYP at predicting the α value for the *C* rotational constant, which is important, as the C_v value largely determines the spacing between bands and plays perhaps the largest role in the initial identification of the $K_a = 0$ series leading to the fitting of the vibrational-state spectrum. This, of course, becomes even more important when the species is in low abundance or otherwise has low transition intensities. The β values presented here are the result of the first documented attempt at a purely computational prediction of these values for larger molecules. Their agreement with the experiment is impressive. Nearly three quarters of the β values are predicted within 50% of their experimental values—a value that is reasonable for the quartic centrifugal distortion constants. (Quartic distortion constants, themselves, are typically reported on the scale of kHz, whereas these predictions are on the scale of Hz.) There are a few exceptions, with several β values being predicted with the wrong sign, but most of the same order of magnitude, e.g., D_J of ν_{17} for [1-^{2}H]-1*H*-1,2,3-triazole, d_1 and d_2 of ν_{18} for [4-^{2}H]-2*H*-1,2,3-triazole, or D_K of ν_{12} for [4,5-^{2}H]-2*H*-1,2,3-triazole. The β value of d_2 for ν_{11} of [2-^{2}H]-2*H*-1,2,3-triazole is predicted to be the opposite sign and an order of magnitude larger than that determined experimentally. This constant is determined from purely high-resolution infrared data without addressing the Coriolis-coupling to ν_9, which may not be an accurate experimental determination. Overall, the ability of the novel technique for predicting excited-state quartic centrifugal distortion constants may be deemed successful.

The satisfactory performance of the partial-VPT4 quartic distortion constants may be related to the fact that the majority of the neglected perturbation products in our implementation are those that involve the rigid-rotor Hamiltonian one or more times. The importance of the anharmonic potential is unrelated to the size of the molecule, e.g., the anharmonicity of a C–H or N–H stretch is similar regardless of where it is found. Typical values of rotational constants, however, span several orders of magnitude, depending on the size of the molecule. The relative importance of the rigid-rotor and the anharmonic potential operators should be a function of the system size; thus, the VPT constants of larger molecules (around triazole's size) will tend to be dominated by anharmonic potential

TABLE VIII. Experimental and computational vibrational frequencies (cm^{-1}) for 2*H*-1,2,3-triazole and [2-^{2}H]-2*H*-1,2,3-triazole.

	2*H*-1,2,3-triazole			
	Symmetry	B3LYP	CCSD(T)	Expt.
ν_{12}	B_1	521	532	532.934 421 6 (20)
ν_9	A_2	670	667	
ν_{11}	B_1	706	709	706.514 423 1 (30)
ν_{10}	B_1	822	828	825.627 151 4 (53)
ν_8	A_2	876	880	
	[2-^{2}H]-2*H*-1,2,3-triazole			
		B3LYP	CCSD(T)	Expt.
ν_{12}	B_1	409	421	420.969 173 1 (29)
ν_9	A_2	671	668	
ν_{11}	B_1	672	671	668.908 825 9 (50)
ν_{10}	B_1	820	826	823.126 791 3 (70)
ν_8	A_2	875	836	

effects. Our current implementation does not neglect any contributions from the anharmonic potential, which may explain its success for this application.

Table VIII shows the B3LYP and CCSD(T) predicted fundamental frequencies for the five lowest-energy fundamental states of 2*H*- and [2-^{2}H]-2*H*-1,2,3-triazole compared with the values for ν_{12}, ν_{11}, and ν_{10} determined in this work. Previously, low-resolution vapor phase measurements were reported for 1,2,3-triazole, though the transitions were assigned to 1*H*-1,2,3-triazole rather than 2*H*-1,2,3-triazole.[38] For both isotopologues, CCSD(T) energies of ν_{12} (out-of-plane N–H wag) are in much closer agreement with the experimental value than the B3LYP energies. The two levels of theory are nearly indistinguishable in their abilities to predict the energies of ν_{11} and ν_{10} for both isotopologues.

CONCLUSION

The variety of vibrationally excited states and isotopologues observed in this work enables a comparison of the spectroscopic constants, and changes in them, across the different species. The combination of our unique dataset, in conjunction with the new computational methodology, permits us to provide an informed evaluation of various strategies that are often employed in the analysis of rotational spectra. A common practice is to use experimental spectroscopic constants from an analogous species (a better-characterized isotopologue or the ground state) as a substitute for indeterminable constants for a species of interest. This practice is based upon the assumption that the substitute value represents a better approximation of the true value of the constant of interest than simply fixing the value at zero (as is commonly done). An alternative approach is to substitute a computationally predicted value of the constant, which is feasible in some circumstances but not in others (*vide infra*). This study provides a way to probe whether the corresponding ground-state value of that isotopologue, or the same vibrationally excited state in a different isotopologue, is a better substitute for a centrifugal distortion constant of a vibrationally excited specie. The spectroscopic constants determined for 1,2,3-triazole reveal that there is not a consistent change from ground to analogous vibrational state that can be applied across isotopologues. In fact, some changes have different signs and magnitudes for analogous vibrational modes. This is not surprising, given the large impact of H/D substitution on the position of principle axes and force constants that affect the centrifugal distortion constants. As expected, changes from ground to excited states tend to be smaller than changes in spectroscopic constants between isotopologues. If no computational prediction of the excited-state distortion terms is available, the less risky substitute is the corresponding value of the ground state for that isotopologue.

Historically, computational predictions for excited-state centrifugal distortion constants have not been available to spectroscopists. Using the new computational methodology described in this study, provisional computational predictions for excited-state centrifugal distortion constants are available (with a complete VPT4 treatment soon to be implemented). This development enables us to probe the validity of the common practice of substituting ground-state distortion constants for their excited-state counterparts. For the centrifugal distortion terms of some of the vibrational states encountered in the current study, such as d_1 of ν_{18} of [4,5-^{2}H]-1*H*-1,2,3-triazole, calculations indicate that the distortion constant changes sign compared with the ground state. This reveals that the otherwise best predictor of the excited-state distortion constant—the corresponding ground-state value—is less than ideal and may result in a less accurate *a priori* prediction of the spectrum. The availability of computational methodology that accurately predicts the value of the excited-state term, such as d_1 of ν_{18} of [4,5-^{2}H]-1*H*-1,2,3-triazole, enables a better modeling of the rotational spectrum, because terms held constant within a set, e.g., quartic, sextic, of centrifugal distortion terms have a substantial effect on the fitted terms. More accurately predicted terms that cannot be determined experimentally result in a more physically meaningful and accurate determination of the terms that can be fit. While using ground-state constants is not a substantial barrier to predicting and fitting vibrational states that can be treated by a single-state Hamiltonian, it can be a limitation for the accurate determination of spectroscopic constants for vibrationally excited states that exhibit Coriolis coupling. Additionally, the more accurate the determined constants, the better they are able to extrapolate outside the observed frequency region and the more accurate the information that these terms provide about the structure of the molecule.

SUPPLEMENTARY MATERIAL

High-resolution infrared data collection parameters, least-squares fitting files for all isotopologues, data distribution plots for all isotopologues, and computational output files are provided in the supplementary material.

ACKNOWLEDGMENTS

We gratefully acknowledge funding from the National Science Foundation for support of this project (R.J.M. Grant No.

CHE-1954270 and J.F.S. Grant No. CHE-1664325). Part of the research described in this paper was performed at the Canadian Light Source, a national research facility of the University of Saskatchewan, which is supported by the Canada Foundation for Innovation (CFI), the Natural Sciences and Engineering Research Council (NSERC), the National Research Council (NRC), the Canadian Institutes of Health Research (CIHR), the Government of Saskatchewan, and the University of Saskatchewan. We thank Michael McCarthy for the loan of an amplification-multiplication chain and the Harvey Spangler Award (to B.J.E.) for funding that supported the purchase of the corresponding detector.

AUTHOR DECLARATIONS

Conflict of Interest

The authors have no conflicts to disclose.

Author Contributions

Maria A. Zdanovskaia: Formal analysis (equal); Investigation (equal); Writing – original draft (equal); Writing – review & editing (equal). **Peter R. Franke**: Formal analysis (equal); Software (equal); Writing – original draft (supporting); Writing – review & editing (equal). **Brian J. Esselman**: Conceptualization (equal); Formal analysis (equal); Investigation (equal); Writing – original draft (equal); Writing – review & editing (equal). **Brant E. Billinghurst**: Formal analysis (equal); Funding acquisition (equal); Investigation (equal); Writing – original draft (supporting); Writing – review & editing (equal). **Jianbao Zhao**: Formal analysis (equal); Investigation (equal); Writing – original draft (supporting); Writing – review & editing (equal). **John F. Stanton**: Formal analysis (equal); Funding acquisition (equal); Investigation (equal); Software (equal); Supervision (equal); Writing – review & editing (equal). **R. Claude Woods**: Conceptualization (equal); Formal analysis (equal); Investigation (equal); Supervision (equal); Writing – review & editing (equal). **Robert J. McMahon**: Funding acquisition (equal); Supervision (equal); Writing – review & editing (equal).

DATA AVAILABILITY

The data that support the findings of this study are available within the article and its supplementary material.

REFERENCES

[1]W. Gordy and R. Cook, *Microwave Molecular Spectra*, 3rd ed. (Wiley-Interscience, New York, 1984), Vol. 18.
[2]L. E. Snyder, "Molecules in space," in *MTP International Review of Science: Physical Chemistry, Series One*, edited by D. A. Ramsay (Butterworth, 1972), Vol. 3, pp. 193–240.
[3]G. Winnewisser, E. Churchwell, and C. Walmsley, "Astrophysics of interstellar molecules," in *Modern Aspects of Microwave Spectroscopy*, edited by G. W. Chantry (Academic Press, 1979), pp. 313–503.
[4]R. L. Cook, "Microwave molecular spectroscopy," in *Encyclopedia of Physical Science and Technology*, 3rd ed., edited by R. A. Meyers (Academic Press, New York, 2003), pp. 799–852.
[5]J. K. G. Watson, "Determination of centrifugal distortion coefficients of asymmetric-top molecules," J. Chem. Phys. **46**, 1935–1949 (1967).
[6]J. K. G. Watson, "Determination of centrifugal distortion coefficients of asymmetric-top molecules. III. Sextic coefficients," J. Chem. Phys. **48**, 4517–4524 (1968).
[7]I. M. Mills, "Vibration-rotation structure in asymmetric- and symmetric-top molecules," in *Molecular Spectroscopy: Modern Research*, edited by K. N. Rao and C. W. Mathews (Academic Press, New York, 1972), Vol. 1, pp. 115–140.
[8]P. M. Dorman, B. J. Esselman, R. C. Woods, and R. J. McMahon, "An analysis of the rotational ground state and lowest-energy vibrationally excited dyad of 3-cyanopyridine: Low symmetry reveals rich complexity of perturbations, couplings, and interstate transitions," J. Mol. Spectrosc. **373**, 111373 (2020).
[9]P. M. Dorman, B. J. Esselman, J. E. Park, R. C. Woods, and R. J. McMahon, "Millimeter-wave spectrum of 4-cyanopyridine in its ground state and lowest-energy vibrationally excited states, ν_{20} and ν_{30}," J. Mol. Spectrosc. **369**, 111274 (2020).
[10]M. A. Zdanovskaia, B. J. Esselman, H. S. Lau, D. M. Bates, R. C. Woods, R. J. McMahon, and Z. Kisiel, "The 103–360 GHz rotational spectrum of benzonitrile, the first interstellar benzene derivative detected by radioastronomy," J. Mol. Spectrosc. **351**, 39–48 (2018).
[11]M. A. Zdanovskaia, M.-A. Martin-Drumel, Z. Kisiel, O. Pirali, B. J. Esselman, R. C. Woods, and R. J. McMahon, "The eight lowest-energy vibrational states of benzonitrile: Analysis of Coriolis and Darling-Dennison couplings by millimeter-wave and far-infrared spectroscopy," J. Mol. Spectrosc. **383**, 111568 (2022).
[12]M. A. Zdanovskaia, B. J. Esselman, R. C. Woods, and R. J. McMahon, "The 130–370 GHz rotational spectrum of phenyl isocyanide (C_6H_5NC)," J. Chem. Phys. **151**, 024301 (2019).
[13]L. Pszczółkowski, E. Białkowska-Jaworska, and Z. Kisiel, "The millimeter wave rotational spectrum of lactic acid," J. Mol. Spectrosc. **234**, 106–112 (2005).
[14]Z. Kisiel, O. Dorosh, M. Winnewisser, M. Behnke, I. R. Medvedev, and F. C. De Lucia, "Comprehensive analysis of the FASSST rotational spectrum of $S(CN)_2$," J. Mol. Spectrosc. **246**, 39–56 (2007).
[15]Z. Kisiel, E. B. Jaworska, R. A. H. Butler, D. T. Petkie, P. Helminger, I. R. Medvedev, and F. C. De Lucia, "The rotational spectrum of chlorine nitrate ($ClONO_2$) in the four lowest $n\nu_9$ polyads," J. Mol. Spectrosc. **254**, 78–86 (2009).
[16]Z. Kisiel and A. Kraśnicki, "The millimetre-wave rotational spectrum of phenylacetylene," J. Mol. Spectrosc. **262**, 82–88 (2010).
[17]E. Białkowska-Jaworska, L. Pszczółkowski, and Z. Kisiel, "Comprehensive analysis of the rotational spectrum of 2,2-dichloropropane," J. Mol. Spectrosc. **308-309**, 20–27 (2015).
[18]Z. Kisiel, L. Pszczółkowski, E. Białkowska-Jaworska, M. Jaworski, I. Uriarte, F. J. Basterretxea, and E. J. Cocinero, "Rotational spectroscopy update for the newly identified atmospheric ozone depleter CF_3CCl_3," J. Mol. Spectrosc. **352**, 1–9 (2018).
[19]J. K. G. Watson, "Higher-order vibration-rotation energies of the X_3 molecule," J. Mol. Spectrosc. **103**, 350–363 (1984).
[20]M. R. Aliev, "Vibrational dependence of the quartic centrifugal constant and the octic centrifugal constant of linear molecules," Opt. Spectrosc. **60**, 411–412 (1986).
[21]V. Tyuterev, S. Tashkun, and H. Seghir, "High-order contact transformations: General algorithm, computer implementation, and triatomic tests," Proc. SPIE **5311**, 164–175 (2004).
[22]J. K. G. Watson, "The vibrational dependence of quartic centrifugal distortion," J. Mol. Struct. **742**, 91–98 (2005).
[23]J. Demaison, L. Margulès, and J. E. Boggs, "Equilibrium structure and force field of NH_2," Phys. Chem. Chem. Phys. **5**, 3359–3363 (2003).
[24]L. Margulès, R. A. Motiyenko, and J. Demaison, "Millimeterwave and submillimeterwave spectra of sulfur dioxide $^{32}S^{16}O^{18}O$ and $^{32}S^{18}O_2$, centrifugal distortion analysis and equilibrium structure," J. Quant. Spectrosc. Radiat. Transfer **253**, 107153 (2020).
[25]V. Tyuterev, S. Tashkun, M. Rey, and A. Nikitin, "High-order contact transformations of molecular Hamiltonians: General approach, fast computational algorithm and convergence of ro-vibrational polyad models," Mol. Phys. **120**, e2096140 (2022).
[26]M. A. Zdanovskaia, B. J. Esselman, S. M. Kougias, B. K. Amberger, J. F. Stanton, R. C. Woods, and R. J. McMahon, "Precise equilibrium structures of 1*H*- and 2*H*-1,2,3-Triazoles ($C_2H_3N_3$) by millimeter-wave spectroscopy," J. Chem. Phys. **157**, 084305 (2022).

[27]G. Rauhut, "Modulation of reaction barriers by generating reactive intermediates: Double proton transfer reactions," Phys. Chem. Chem. Phys. **5**, 791–800 (2003).
[28]Z. Zhou, R. Liu, J. Wang, S. Li, M. Liu, and J.-L. Brédas, "Intra- and intermolecular proton transfer in 1*H*(2*H*)-1,2,3-triazole based systems," J. Phys. Chem. A **110**, 2322–2324 (2006).
[29]J.-L. M. Abboud, C. Foces-Foces, R. Notario, R. E. Trifonov, A. P. Volovodenko, V. A. Ostrovskii, I. Alkorta, and J. Elguero, "Basicity of *N*-H- and *N*-methyl-1,2,3-triazoles in the gas phase, in solution, and in the solid state—An experimental and theoretical study," Eur. J. Org. Chem. **2001**, 3013–3024.
[30]F. Tomas, J. L. M. Abboud, J. Laynez, R. Notario, L. Santos, S. O. Nilsson, J. Catalan, R. M. Claramunt, and J. Elguero, "Tautomerism and aromaticity in 1,2,3-triazoles: The case of benzotriazole," J. Am. Chem. Soc. **111**, 7348–7353 (1989).
[31]J. Catalán, M. Sánchez-Cabezudo, J. L. G. De Paz, J. Elguero, R. W. Taft, and F. Anvia, "The tautomerism of 1,2,3-triazole, 3(5)-methylpyrazole and their cations," J. Comput. Chem. **10**, 426–433 (1989).
[32]M. Begtrup, C. J. Nielsen, L. Nygaard, S. Samdal, C. E. Sjøgren, and G. O. Sørensen, "The molecular structure and tautomer equilibrium of gaseous 1,2,3-triazole studied by microwave spectroscopy, electron diffraction and *ab initio* calculations," Acta Chem. Scand., Ser. B **42**, 500–514 (1988).
[33]G. L. Blackman, R. D. Brown, F. R. Burden, and W. Garland, "Nuclear quadrupole coupling in the microwave spectrum of 1,2,3-triazole," J. Mol. Spectrosc. **65**, 313–318 (1977).
[34]G. O. Sorensen, L. Nygaard, and M. Begtrup, "Microwave spectrum of 1-deuterio-1,2,3-triazole," J. Chem. Soc., Chem. Commun. **1974**, 605–606.
[35]O. L. Stiefvater, H. Jones, and J. Sheridan, "Double-resonance-double-search assignment of the microwave spectrum of 1,2,3-triazole," Spectrochim. Acta, Part A **26**, 825–833 (1970).
[36]S. G. Aziz, S. A. Elroby, A. Alyoubi, O. I. Osman, and R. Hilal, "Experimental and theoretical assignment of the vibrational spectra of triazoles and benzotriazoles. Identification of IR marker bands and electric response properties," J. Mol. Model. **20**, 2078 (2014).
[37]F. Billes, H. Endrédi, and G. Keresztury, "Vibrational spectroscopy of triazoles and tetrazole," J. Mol. Struct.: THEOCHEM **530**, 183–200 (2000).
[38]E. Borello, A. Zecchina, and E. Guglielminotti, "A vibrational assignment for 1,2,3-triazole," J. Chem. Soc. B **1969**, 307–311.
[39]S. A. Kudchadker and C. N. R. Rao, "Infrared spectra and normal vibrations of isomeric triazoles," Indian J. Chem. **11**, 140–142 (1973).
[40]P. M. Higgins, B. J. Esselman, M. A. Zdanovskaia, R. C. Woods, and R. J. McMahon, "Millimeter-wave spectroscopy of the chlorine isotopologues of chloropyrazine and twenty-two of their vibrationally excited states," J. Mol. Spectrosc. **364**, 111179 (2019).
[41]B. J. Esselman, M. A. Zdanovskaia, R. C. Woods, and R. J. McMahon, "Millimeter-wave spectroscopy of the chlorine isotopologues of 2-chloropyridine and twenty-three of their vibrationally excited states," J. Mol. Spectrosc. **365**, 111206 (2019).
[42]Z. Kisiel, E. Białkowska-Jaworska, and L. Pszczółkowski, "The rotational spectrum of $CBrClF_2$ (Halon BCF): II. The lowest excited vibrational states and nuclear quadrupole coupling tensors," J. Mol. Spectrosc. **185**, 71–78 (1997).
[43]Z. Kisiel, E. Białkowska-Jaworska, and L. Pszczółkowski, "The ∠ICI bending satellites in the millimeter-wave rotational spectra of CH_2I_2 and CD_2I_2," J. Mol. Spectrosc. **199**, 5–12 (2000).
[44]R. A. H. Butler, D. T. Petkie, P. Helminger, F. C. De Lucia, E. Bialkowska-Jaworska, and Z. Kisiel, "The millimeter-wave spectrum of chlorine nitrate ($ClONO_2$): The ν_6 vibrational state," J. Mol. Spectrosc. **244**, 113–116 (2007).
[45]R. A. H. Butler, D. T. Petkie, P. Helminger, F. C. De Lucia, and Z. Kisiel, "The rotational spectrum of chlorine nitrate ($ClONO_2$): The $\nu_5/\nu_6\nu_9$ dyad," J. Mol. Spectrosc. **243**, 1–9 (2007).
[46]O. Dorosh, E. Białkowska-Jaworska, Z. Kisiel, and L. Pszczółkowski, "New measurements and global analysis of rotational spectra of Cl-, Br-, and I-benzene: Spectroscopic constants and electric dipole moments," J. Mol. Spectrosc. **246**, 228–232 (2007).
[47]A. Kraśnicki, Z. Kisiel, B. J. Drouin, and J. C. Pearson, "Terahertz spectroscopy of isotopic acrylonitrile," J. Mol. Struct. **1006**, 20–27 (2011).
[48]Z. Kisiel, E. Białkowska-Jaworska, J. Chen, L. Pszczółkowski, P. Gawryś, and J. Kosarzewski, "Rotational spectroscopy and precise molecular structure of 1,2-dichlorobenzene," J. Mol. Spectrosc. **374**, 111380 (2020).
[49]B. J. Esselman, B. K. Amberger, J. D. Shutter, M. A. Daane, J. F. Stanton, R. C. Woods, and R. J. McMahon, "Rotational spectroscopy of pyridazine and its isotopologs from 235–360 GHz: Equilibrium structure and vibrational satellites," J. Chem. Phys. **139**, 224304 (2013).
[50]G. Wlodarczak, J. Demaison, B. P. van Eijck, M. Zhao, and J. E. Boggs, "*Ab initio* and experimental quartic centrifugal distortion constants of acetone, pyrazole, and γ-pyrone," J. Chem. Phys. **94**, 6698–6707 (1991).
[51]L. Nygaard, D. Christen, J. T. Nielsen, E. J. Pedersen, O. Snerling, E. Vestergaard, and G. O. Sørensen, "Microwave spectra of isotopic pyrazoles and molecular structure of pyrazole," J. Mol. Struct. **22**, 401–413 (1974).
[52]W. H. Kirchhoff, "The microwave spectrum and dipole moment of pyrazole," J. Am. Chem. Soc. **89**, 1312–1316 (1967).
[53]B. K. Amberger, B. J. Esselman, J. F. Stanton, R. C. Woods, and R. J. McMahon, "Precise equilibrium structure determination of hydrazoic acid (HN_3) by millimeter-wave spectroscopy," J. Chem. Phys. **143**, 104310 (2015).
[54]Z. Kisiel, L. Pszczółkowski, B. J. Drouin, C. S. Brauer, S. Yu, J. C. Pearson, I. R. Medvedev, S. Fortman, and C. Neese, "Broadband rotational spectroscopy of acrylonitrile: Vibrational energies from perturbations," J. Mol. Spectrosc. **280**, 134–144 (2012).
[55]Z. Kisiel, L. Pszczółkowski, I. R. Medvedev, M. Winnewisser, F. C. De Lucia, and E. Herbst, "Rotational spectrum of *trans–trans* diethyl ether in the ground and three excited vibrational states," J. Mol. Spectrosc. **233**, 231–243 (2005).
[56]Z. Kisiel and E. Białkowska-Jaworska, "Sextic centrifugal distortion in fluorobenzene and phenylacetylene from cm-wave rotational spectroscopy," J. Mol. Spectrosc. **359**, 16–21 (2019).
[57]H. M. Pickett, "The fitting and prediction of vibration-rotation spectra with spin interactions," J. Mol. Spectrosc. **148**, 371–377 (1991).
[58]Z. Kisiel, "Assignment and analysis of complex rotational spectra," in *Spectroscopy From Space*, edited by J. Demaison, K. Sarka, and E. A. Cohen (Kluwer Academic Publishers, Dordrecht, 2001), pp. 91–106, http://www.ifpan.edu.pl/~kisiel/prospe.htm.
[59]PROSPE—Programs for ROtational SPEctroscopy, http://info.ifpan.edu.pl/~kisiel/prospe.htm.
[60]M. J. Frisch, G. W. Trucks, H. B. Schlegel, G. E. Scuseria, M. A. Robb, J. R. Cheeseman, G. Scalmani, V. Barone, G. A. Petersson, H. Nakatsuji, X. Li, M. Caricato, A. V. Marenich, J. Bloino, B. G. Janesko, R. Gomperts, B. Mennucci, H. P. Hratchian, J. V. Ortiz, A. F. Izmaylov, J. L. Sonnenberg, D. Williams-Young, F. Ding, F. Lipparini, F. Egidi, J. Goings, B. Peng, A. Petrone, T. Henderson, D. Ranasinghe, V. G. Zakrzewski, J. Gao, N. Rega, G. Zheng, W. Liang, M. Hada, M. Ehara, K. Toyota, R. Fukuda, J. Hasegawa, M. Ishida, T. Nakajima, Y. Honda, O. Kitao, H. Nakai, T. Vreven, K. Throssell, J. A. Montgomery, Jr., J. E. Peralta, F. Ogliaro, M. J. Bearpark, J. J. Heyd, E. N. Brothers, K. N. Kudin, V. N. Staroverov, T. A. Keith, R. Kobayashi, J. Normand, K. Raghavachari, A. P. Rendell, J. C. Burant, S. S. Iyengar, J. Tomasi, M. Cossi, J. M. Millam, M. Klene, C. Adamo, R. Cammi, J. W. Ochterski, R. L. Martin, K. Morokuma, O. Farkas, J. B. Foresman, and D. J. Fox, GAUSSIAN 16, Revision B.01, Gaussian, Inc., Wallingford, CT, 2016.
[61]M. J. O. Deegan and P. J. Knowles, "Perturbative corrections to account for triple excitations in closed and open shell coupled cluster theories," Chem. Phys. Lett. **227**, 321–326 (1994).
[62]C. Hampel, K. A. Peterson, and H.-J. Werner, "A comparison of the efficiency and accuracy of the quadratic configuration interaction (QCISD), coupled cluster (CCSD), and Brueckner coupled cluster (BCCD) methods," Chem. Phys. Lett. **190**, 1–12 (1992).
[63]K. Raghavachari, G. W. Trucks, J. A. Pople, and M. Head-Gordon, "A fifth-order perturbation comparison of electron correlation theories," Chem. Phys. Lett. **157**, 479–483 (1989).
[64]J. F. Stanton, "Why CCSD(T) works: A different perspective," Chem. Phys. Lett. **281**, 130–134 (1997).
[65]J. F. Stanton, J. Gauss, M. E. Harding, and P. G. Szalay, CFOUR, Coupled-Cluster Techniques for Computational Chemistry, with contributions from A. A. Auer, R. J. Bartlett, U. Benedikt, C. Berger, D. E. Bernholdt, Y. J. Bomble, L. Cheng, O. Christiansen, M. Heckert, O. Heun, C. Huber, T.-C. Jagau, D. Jonsson, J. Jusélius, K. Klein, W. J. Lauderdale, D. A. Matthews, T. Metzroth, D. P.

O'Neill, D. R. Price, E. Prochnow, K. Ruud, F. Schiffmann, W. Schwalbach, S. Stopkowicz, A. Tajti, J. Vázquez, F. Wang, and J. D. Watts and the integral packages: MOLECULE (J. Almlöf and P. R. Taylor), PROPS (P. R. Taylor), ABACUS (T. Helgaker, H. J. A. Jensen, P. Jørgensen, and J. Olsen), and ECP routines by A. V. Mitin and C. van Wüllen, www.cfour.de.

[66]D. A. Matthews, L. Cheng, M. E. Harding, F. Lipparini, S. Stopkowicz, T.-C. Jagau, P. G. Szalay, J. Gauss, and J. F. Stanton, "Coupled-cluster techniques for computational chemistry: The CFOUR program package," J. Chem. Phys. **152**, 214108 (2020).

[67]J. Almlöf and P. R. Taylor, "General contraction of Gaussian basis sets. I. Atomic natural orbitals for first- and second-row atoms," J. Chem. Phys. **86**, 4070–4077 (1987).

[68]T. H. Dunning, Jr., "Gaussian basis sets for use in correlated molecular calculations. I. The atoms boron through neon and hydrogen," J. Chem. Phys. **90**, 1007–1023 (1989).

[69]K. A. Peterson and T. H. Dunning, Jr., "Accurate correlation consistent basis sets for molecular core–valence correlation effects: The second row atoms Al–Ar, and the first row atoms B–Ne revisited," J. Chem. Phys. **117**, 10548–10560 (2002).

[70]D. E. Woon and T. H. Dunning, Jr., "Gaussian basis sets for use in correlated molecular calculations. V. Core-valence basis sets for boron through neon," J. Chem. Phys. **103**, 4572–4585 (1995).

[71]P. R. Franke, J. F. Stanton, and G. E. Douberly, "How to VPT2: Accurate and intuitive simulations of CH stretching infrared spectra using VPT2+K with large effective Hamiltonian resonance treatments," J. Phys. Chem. A **125**, 1301–1324 (2021).

[72]W. H. Green, D. Jayatilaka, A. Willetts, R. D. Amos, and N. C. Handy, "The prediction of spectroscopic properties from quartic correlated force fields: HCCF, HFCO, SiH_3^+," J. Chem. Phys. **93**, 4965–4981 (1990).

[73]Mathematica, version 12.9, Wolfram Research, Inc., Champaign, IL, 2020.

[74]A. M. Rosnik and W. F. Polik, "VPT2+K spectroscopic constants and matrix elements of the transformed vibrational Hamiltonian of a polyatomic molecule with resonances using Van Vleck perturbation theory," Mol. Phys. **112**, 261–300 (2014).

[75]H. Schneider, K. M. Vogelhuber, F. Schinle, J. F. Stanton, and J. M. Weber, "Vibrational spectroscopy of nitroalkane chains using electron autodetachment and Ar predissociation," J. Phys. Chem. A **112**, 7498–7506 (2008).

[76]M. R. Aliev and J. K. G. Watson, "Calculated sextic centrifugal distortion constants of polyatomic molecules," J. Mol. Spectrosc. **61**, 29–52 (1976).

[77]M. R. Aliev and J. K. G. Watson, "Higher-order effects in the vibration–rotation spectra of semirigid molecules," in *Molecular Spectroscopy: Modern Research*, edited by K. N. Rao (Academic Press, Orlando, FL, 1985), Vol. 3, pp. 1–67.

[78]C. Georghiou, "Sextic centrifugal distortion constants of polyatomic molecules," Mol. Phys. **32**, 1279–1290 (1976).